A combined microRNA and target protein-based panel for predicting the probability and severity of uremic vascular calcification: a translational study

Chia-Ter Chao[1,2,3], Hsiang-Yuan Yeh[4], You-Tien Tsai[1], Chih-Kang Chiang[2,5], Huei-Wen Chen[2]

[1]Division of Nephrology, Department of Medicine, National Taiwan University Hospital Bei-Hu Branch, Taipei, Taiwan

[2]Graduate Institute of Toxicology; [3]Department of Internal Medicine, National Taiwan University College of Medicine, Taipei 10051, Taiwan

[4]School of Big Data Management, Soochow University, Taipei, Taiwan

[5]Department of Integrative Diagnostics and Therapeutics, National Taiwan University Hospital, Taipei, Taiwan

Correspondence to: Professor Huei-Wen Chen; Graduate Institute of Toxicology, National Taiwan University; No.1, Section 4, Ren-Ai Road, Zhong-Zhen District, Taipei, Taiwan; Email: shwchen@ntu.edu.tw

Running title: microRNA-protein pair for evaluating uremic VC

Category: Original investigation

Word Count: 9000

Abstract

Aims: Vascular calcification (VC) increases the future risk of cardiovascular events in uremic patients, but effective therapies are still unavailable. Accurate identification of those at risk of developing VC using pathogenesis-based biomarkers is of particular interest and may facilitate individualized risk stratification. We aimed to uncover miRNA-target protein-based biomarker panels for evaluating uremic VC probability and severity.

Methods and Results: We created a 3-tiered *in vitro* VC model and an *in vivo* uremic rat model receiving high phosphate diet to mimic uremic VC. RNAs from the 3-tiered *in vitro* and *in vivo* uremic VC models underwent miRNA and mRNA microarray, with results screened for differentially expressed miRNAs and their target genes as biomarkers. Findings were validated in original models and additionally in an *ex vivo* VC model and human cells, followed by functional assays of identified miRNAs and target proteins, and tests of sera from end-stage renal disease (ESRD) and non-dialysis dependent chronic kidney disease (CKD) patients without and with VC. Totally 122 down-regulated and 119 up-regulated miRNAs during calcification progression were identified initially; further list-narrowing based on miRNA-mRNA pairing, anti-correlation, and functional enrichment left 16 and 14 differentially expressed miRNAs and mRNAs. Levels of 4 miRNAs (miR-10b-5p, miR-195, miR-125b-2-3p, and miR-378a-3p) were shown to decrease throughout all models tested, while 1 mRNA (SULF1, a potential target of miR-378a-3p) exhibited the opposite trend

concurrently. Among 96 ESRD (70.8% with VC) and 59 CKD patients (61% with VC), serum miR-125b2-3p and miR-378a-3p decreased with greater VC severity, while serum SULF1 levels increased. Adding serum miR-125b-2-3p, miR-378a-3p, and SULF1 into regression models for VC substantially improved performance compared to using clinical variables alone.

Conclusion: Using a translational approach, we discovered a novel panel of biomarkers for gauging the probability/severity of uremic VC based on miRNAs/target proteins, which improved the diagnostic accuracy.

Translational perspective: Through miRNA and transcriptomic profiling with serial result validation in different models, we discover that miR-378a-3p and its target gene, *SULF1*, are an important pair of circulating biomarkers for the diagnosis and severity classification of uremic VC among patients with non-dialysis CKD and ESRD. This approach improves the predictive performance compared to that based on traditional clinical features alone. These findings suggest that a combined miRNA/target protein panel may represent a potentially useful approach for detecting uremic VC.

Keywords: chronic kidney disease-mineral bone disorder; end-stage renal disease; hemodialysis; microRNA; vascular calcification

Abbreviations

AAC: aortic arch calcification; ALP: alkaline phosphatase; ASMC: aortic smooth muscle cell; ATCC: American type culture collection; AUROC: area under the receiver-operating characteristics curve; BMP, bone morphogeneic protein; BP: biological process; CCK-8: cell counting kit-8; CEL: cell intensity file; CI: confidence interval; CKD: chronic kidney disease; CKD-MBD: chronic kidney disease-mineral bone disorder; DEMi: differentially expressed microRNA; DM: diabetes mellitus; ELISA: enzyme-linked immunosorbent assay; ESRD: end-stage renal disease; FBS: fetal bovine sera; FDR: false discovery rate; FGF: fibroblast growth factor; GAPDH: glyceraldehyde 3-phosphate dehydrogenase; GO: gene ontology; HIF: hypoxia-inducible factor; HP: high phosphate; IS: indoxyl sulfate; KEGG: Kyoto encyclopedia of genes and genomes; LNA: locked nucleic acid; MDRD: Modification of Diet in Renal Disease; MF: molecular function; miRNA: microRNA; OR: odds ratio; PPI: protein-protein interaction; qPCR: quantitative polymerase chain reaction; RIN: RNA integrity number; RT: reverse transcription; SNP: single nucleotide polymorphism; TNF: tumor necrosis factor; VC: vascular calcification; VSMC: vascular smooth muscle cell

1. INTRODUCTION

Vascular calcification (VC), a prognostically important complication on the spectrum of chronic kidney disease-mineral bone disorders (CKD-MBDs), is highly prevalent among patients with CKD. A recent meta-analysis of 38 studies estimated that VC occurred in 59% (49% - 69%) and 65% (55% - 75%) of pre-dialysis CKD and hemodialysis-dependent end-stage renal disease (ESRD) patients, respectively.[1] Age and prolonged duration undergoing chronic dialysis are established risk factors for developing VC, and other features including diabetes mellitus (DM), deregulated divalent ion balance, vitamins K and D deficiencies, and secondary hyperparathyroidism have all been implicated to increase the risk of uremic VC.[2,3] CKD patients who develop incident or aggravated VC are at an increased risk of renal functional decline, cardiovascular events, and elevated mortality.[4,5] Despite the perceived importance of VC outcomes, effective therapies against this dreadful CKD complication are still unavailable, presumably stemming from an inadequate understanding of the complex pathophysiology involved.[3,6] More importantly, the failure of existing VC therapies can result from ineffective identification of candidate patients at pathophysiologically greater risk of worsening VC.[7] This renders the accurate targeting of CKD patients at higher risk of developing VC using molecular biomarkers based on VC pathogenesis of potential interest.

The pathogenesis of uremic VC, particularly the medial type, has evolved from traditional passive calcium deposition in vascular walls to active osteoblast-like matrix secretion by trans-differentiated vascular smooth muscle cells (VSMCs) upon high phosphate (HP) exposure.[8] This phenomenon is further augmented by a downplay of anti-calcific molecules (matrix Gla protein, pyrophosphate, fetuin-A), the rising risk of vascular wall constituent apoptosis, and uremic milieu such as pro-inflammatory status and oxidative stress.[9,10] Epigenetic changes, particularly microRNA (miRNA), have recently been found to play an integral role in uremic VC.[11] Apart from exerting regulatory influences on disease pathogenesis, miRNAs also serve as excellent biomarkers due to their established stability in biologic fluids and their specificity for pathophysiologically relevant diseases.[12,13] Prior studies similarly showed that circulating miRNAs predict cardiovascular diseases much earlier than biochemical markers, including in heart failure and myocardial infarction.[14] Our work previously demonstrated that circulating miRNAs were non-invasive, effective biomarkers for predicting uremic VC worsening over time, an advantage over existing protein-based markers in the field of vascular pathologies.[15] However, whether miRNAs in combination with protein-based biomarkers further improve the disease predictive efficacy compared to each component alone remains unclear. Preliminary oncology studies show that a combined panel of serum proteins and miRNAs exhibit better sensitivity and specificity for the identification of prostate cancer than clinical features alone.[16] None of the existing studies

addresses the utility of circulating miRNAs and proteins for estimating the probability of VC in uremic settings. We therefore designed a series of *in vitro*, *in vivo*, and *ex vivo* experiments to mimic the pathophysiology of uremic VC, followed by miRNA and mRNA profiling to select potentially useful biomarkers. Our experimental findings were validated using sera from patients with non-dialysis dependent CKD and dialysis-dependent ESRD for establishment of the clinical utility of candidate biomarkers identified.

2. MATERIALS AND METHODS

2.1 Reagents, antibodies, and cells

In this study, we used rat aortic vascular smooth muscle cells (VSMCs) A7r5 from the American Type Culture Collection (ATCC), and two types of human aortic smooth muscle cells (ASMCs) from ATCC (PCS-100-012) and Sigma Aldrich (SI-354-05A-1EA), respectively, with previously confirmed phenotypes.[15] All *in vitro* experiments were performed with biologic triplicates except stated otherwise. Indoxyl sulfate (IS) (NO. I3875, Sigma-Aldrich, St. Louis, MI, USA), 1,25-dihydroxy-vitamin D (1,25-$(OH)_2$-D) (NO. 17944, Sigma-Aldrich) (subsequently referred as VitD), and tumor necrosis factor-α (TNF-α) (NO. 510-RT-010, R&D Systems, MN, USA) were obtained from commercial sources of analytical grade. Alizarin red used in calcification staining were bought from Sigma-Aldrich (NO. A5533). For western blotting, primary antibodies against Sulf1, Myoz2, and ß-actin

were from Abnova (1:1000 dilution, PAB8523), Santa Cruz (1:1000 dilution, sc-373876), and NOVUS (NB600-501), respectively, followed by goat anti-rabbit secondary antibodies (1:5000 dilution, HAF008; R&D Systems).

2.2 Establishment of 3-tiered in vitro *calcification models*

We previously harnessed a HP-induced VSMC bio-mineralization model with the purpose of mimicking phosphate-induced uremic VC.[15] The details of model construction are provided in the supplemental method. To further simulate the complex pathophysiology of uremic VC, we created another 3 uremic VC models in addition to the original HP-induced one. Osteogenic media were supplemented with different concentrations of VitD, TNF-α, and IS to represent the dysregulated mineral-regulating hormonal milieu, chronic inflammation, and uremic environment, respectively. We selected optimal concentrations and durations of HP exposure for rat aortic VSMCs, and escalated such stimuli for subsequent microarray analyses and results validation. Findings from calcified and non-calcified rat aortic VSMCs subjected to microarray analysis were validated in HP-treated human ASMCs as well.

2.3 Animal models of uremic VC and ex vivo *organ culture model*

The animal treatment protocol was approved by the Institutional Animal Care and Use committee of the National Taiwan University College of Medicine (NO. 20160400). All

procedures of animal experiments conformed to the National Institute of Health Guide for the Care and Use of Laboratory animals. Eight-week old Sprague-Dawley rats (n = 18) were bought from LASCO (Taichung, Taiwan), acclimatized in the experimental animal center of the National Taiwan University College of Medicine for 1 week, and were then assigned randomly and equally to the control group (standard chow, n = 6), high adenine diet (0.75% adenine; CKD group, n = 6), and high adenine with HP diet (0.75% adenine with 1.2% phosphate; CKD+HP group, n = 6). Animals were given food and water *ad libitum* and housed in a standardized care environment, with body weight and amount of chow intake recorded weekly. After 12 weeks, they were sacrificed by CO_2 anesthesia, followed by serum collection by cardiac puncture, and kidneys and aorta were harvested. Aortas were mechanically stripped of adventitia and endothelial layers. Sera were sent for creatinine, calcium, and phosphate analysis, with the remainder stored for miRNA extraction. Kidneys and aortas were subjected to histopathologic examination, and subsequent Masson Trichrome stain (for kidneys) and von Kossa stain (for aortas). ImageJ (National Institute of Health, Bethesda, USA) was used to quantify the percentages of positive Von Kossa staining areas for aortas of each group. We further estimated the severity of renal pathological changes and analyzed the correlation between renal pathology and the extent of VC among each group. Scoring of renal pathology was done based on dimensions and criteria summarized from the existing literature[17-19], including 6 dimensions (tubular dilation with epithelial flattening,

tubular atrophy, interstitial fibrosis, tubulointerstitial inflammation, glomerulosclerosis, and Bowman's space dilation). The severity of lesions in each dimension was rated from 1 to 5 (1, minimal or < 1% involvement; 2, slight or 1% ~ 25%; 3, moderate or 26% ~ 50%; 4, moderate to severe or 51% ~ 75%; and 5, severe/high or 76% ~ 100% involvement), with a total kidney injury score between 6 and 30. For aortas, after mechanical stripping of endothelia and adventitia, the aortas were sent for RNA and protein extraction for microarray and results validation.

For *ex vivo* organ culture, rat aortas were incubated in ordinary DMEM and DMEM/High media (Sigma Aldrich, Dorset, UK) supplemented with fetal bovine sera (FBS), and a phosphate concentration of 3 mmol/L by adding NaH_2PO_4 and Na_2HPO_4 (1:2 ratio) at a PH of 7.4, for 1 week.[15] After incubation, tissue slices were retrieved for extracting RNA and protein, and for von Kossa staining in order to observe the extent of calcification.

2.4 miRNA and mRNA microarray

RNAs obtained from aortic VSMCs without and with selected concentrations and durations of graded HP, or HP with escalated calcification stimuli (control, HP, HP+T, HP+D, and HP+I), as well as those from animal aortic media (control, CKD, and CKD+HP) were subjected to miRNA microarray (n = 3 per group) using GeneChip miRNA 3.0 array

(Affymetrix) which contains 19,724 probe sets covering 1733 human miRNAs, 680 rat miRNAs, and 1111 mouse miRNAs, carried out at the Center of Genomic Medicine of the National Taiwan University. Before analysis, the RNA integrity number (RIN) for all samples was greater than 7, and each group contained biologic triplicates. Concurrently, RNA from the 3 animal groups (control, CKD, and CKD+HP) were subjected to GeneChip mRNA microarray (Affymetrix).

2.5 *A stepwise bioinformatic analysis to screen for biomarkers of uremic VC*

For the analysis of microarray experiment results, the standard operating procedures of our bioinformatic team include the check for normality of expressions of all groups and the standardization of results from all probes prior to differential expression identification. The mRNA expression profiles from the 3 groups of tissues (control, CKD, and CKD+HP) and the miRNA expression profiles from the 5 cell groups (control, HP, HP+T, HP+D, and HP+I) were acquired based on the Affymetrix Genechip expression data to generate cell intensity files (CELs). We applied RMA+DABG-All analysis for miRNA levels. The statistical inference requires a processed signal, which is an estimate of the expression measure for every miRNA that can be normalized between arrays. On the other hand, Quantile normalization is the default normalization method in the Robust Multi-array Average procedure, which was primarily designed for analyzing gene expression data from

Affymetrix arrays. There were no data points imputed and all results were based on actual values. We applied the following filter strategies to identify differentially expressed miRNAs during uremic calcification. First, we calculated correlation coefficients for levels of each miRNA between cellular (VSMC) and aortic media levels to screen whether the two datasets were closely related (if $P < 0.05$). We tested for the association between different samples based on the Pearson's product moment correlation coefficient, using the *cor.test()* command to carry out the test of significance. This R package command returns results including the correlation coefficient, the adjustment of the p-value for multiple comparisons using the Holm's method, and the 95% confidence interval of the correlation coefficient. Second, we used the sign test for detecting directional cis-acting changes in expressions as a means to identify adaptive divergence to different calcification stimuli exposure. The sign test is a non-parametric test for examining whether there are more negative or positive values among control and treatment groups of VSMCs (control vs. HP, HP+D, HP+T, or HP+I) or aortic media (control vs. CKD or CKD+HP), after subtracting the expression values of the treatment group with those of the control group.[20] These results were followed by meta-analysis combining P-values of correlation coefficients and sign tests to increase statistical power and ensure robust and accurate conclusion, using the sum of logs (Fisher's methods) to provide a better biological interpretation through characterizing which test contributed to the aggregate analysis.[21] Finally, we further filtered miRNA microarray results

based on combined P-values (< 0.05) and fulfillment of the following criteria: 1) expression exhibited a positive VSMC-aortic media correlation; 2) significantly higher or lower expression in HP than control and in at least one of the escalated calcification stimuli settings (HP+T, HP+D, or HP+I vs. HP) in VSMCs; 3) significantly higher or lower expression in the CKD+HP group than in CKD and control groups in aortic media. We used a log fold-change cutoff threshold of ± 0.8 to identify differentially expressed miRNAs (DEMis) for each group comparison. We selected negatively or positively regulated miRNAs satisfying the above criteria as potential candidate uremic VC biomarkers.

2.6 Combinatorial biomarker prediction and curation of genes as miRNA targets

We used a miRNA-based computational prediction analysis to identify the most prominent miRNA-mRNA interactions. Targets for each miRNA were aggregated using *miRNAtap* database in R version 3.4 using the Bioconductor package, and we obtained the predicted targets for each miRNA using geometric mean aggregation method. miRNA target prediction was accomplished using five databases, including DIANA, Miranda, PicTar, TargetScan, and miRDB, whose approaches of target prediction involve different binding strategies. miRNA-mRNA pairs were deemed authentic if mRNA targets of DEMi were predicted by ≥ 3 databases, and the intersections of all identified mRNAs were recognized as targets for that

DEMi. The list of DEMis was further narrowed through a combination of anti-regulatory relationships between DEMis and miRNA targets using prediction databases.

2.7 Functional enrichment of miRNA targets and miRNA-mRNA interaction network construction

We further analyzed putative targets of DEMis, based on functional enrichment using the Kyoto Encyclopedia of Genes and Genomes (KEGG) and Gene Ontology (GO) databases. We applied MyGene.info (http://mygene.info) to access the gene annotation data through web services. Each gene returns the basic annotations like ID, evidence, GO terms pertinent to the biological process (BP), and molecular function (MF) category. Significantly differentially regulated mRNAs were mapped to Entrez Gene and analyzed using the *clusterProfiler* R package for GO and KEGG term enrichment (*enrichGO* and *enrichKEGG*) function to test if the gene signatures were enriched in specific BPs and pathways. The results of the ranked targets of miRNAs were then utilized as the input to conduct GO enrichment analysis with Bioconductor package *topGO*. We determined the BP terms that were significantly enriched for miRNA targets using a Kolmogorov-Smirnov test. We used hypergeometric testing to annotate genes to BPs, and applied the Benjamini-Hochberg correction method for multiple testing.

We also retrieved lists of key target mRNAs potentially regulated by the candidate DEMis from the protein–protein interaction (PPI) network, using the latest available version of PPI datasets from BIOGRID and STRING for further analysis. For BIOGRID, the curated PPI data, containing 15,352 unique proteins and 281,862 interactions, constituted the parental PPI network, to which functionally enriched target mRNAs identified above were mapped. We detected only first-level interactions between target mRNAs and their neighbors in order to achieve maximum biological significance, since first-level interactions likely form tighter regulatory networks of gene expression. We also apply STRING PPI database to extend the associated network of target mRNAs. It was found that multiple GO categories related to muscle, blood, bone, and immune systems stood out in the PPI network. Finally, we selected DEMis and their functionally annotated/PPI networked mRNAs with close interactions for subsequent validation, since these miRNA-mRNA pairs might potentially serve as biomarkers for uremic VC and assist in improved understanding of the molecular basis of related pathophysiology.

2.8 Reverse transcription (RT), quantitative polymerase chain reaction (qPCR) and western blot

We extracted RNA from harvested VSMCs or animal aortas using QIAZOL lysis reagent (QIAGEN, Valencia, CA, USA). After assuring RNA purity (Nanodrop Spectrophotometers;

ThermoFisher Scientific, Waltham, MA, USA), samples were subjected to RT using a kit from Abcam (Cambridge, UK), followed by SYBR green-based qPCR, with results validated using single predominant peaks as shown by dissociative curves. The primer sequences for genes tested and the RT/qPCR/Western blot methods in this study are shown in Table S1 and the supplemental method, respectively. During the validation of miRNA microarray results, we used the same criteria to validate and select which candidate miRNAs could proceed to the next phase of validation; that is, selected miRNAs need to exhibit significantly higher or lower expression in HP vs. control, plus exhibiting a significantly higher or lower expression in ≥ 1 out of 3 escalated calcification settings (HP+T, HP+D, or HP+I vs. HP), when being validated in the *in vitro* model. Those miRNAs exhibiting the same trend as they did in the microarray results were selected for further validation in the *in vivo* model, followed by testing in the *ex vivo* model and human ASMCs.

2.9 Examine the possibility of detecting extracellular/circulating miRNAs as biomarkers during the calcification progress

Rat and human VSMCs were cultured in control media and the pre-specified HP condition as described above. Six hours before harvesting, culture media were exchanged to serum-free media, followed by the collection of cell pellets and media using centrifugation for RNA extraction. In the *ex vivo* model, we similarly collected cultured aorta and their respective

media after exchange to serum-free condition, and analyzed the expression levels of selected DEMis. In the *in vivo* model, we checked the expression levels of serum miRNAs and compared between groups to observe whether candidate DEMi behaved similarly across different calcification severities.

2.10 Functional characterization of candidate DEMis and their potential mRNA targets in VSMCs

The detailed approach for assessing VSMC phenotypic changes (survival and contractility) and calcification propensity during DEMis and their target gene manipulation is shown in the supplemental method.

2.11 Dual-luciferase reporter gene assay

We cloned the 3'-untranslated region (3'-UTR) and the seed sequence of selected target genes based on candidate DEMis into the multiple cloning sites of pmirGLO vector (Promega; Madison, WI, USA). After seeding, VSMCs were co-transfected with an empty vector (negative control), pmiRGLO with the target gene 3'-UTR, pmiRGLO with the seed sequence flanked by 9 nucleotides, and pmiRGLO with mutated seed region of 3'UTR, using Lipofectamine 3000. Prior to use, all luciferase-bearing vectors were verified by the Sanger sequencing. We then co-transfected VSMCs with construct-bearing plasmids and the mimics

of DEMis, and detected luciferase activity 24 hours after transfection. We calculated results with normalization of *Firefly* luciferase activity from DEMi mimics/3'-UTR, seed region, or mutated vectors to those of the DEMi mimics/empty vectors and *Renilla* luciferase activity.

2.12 Assembly of two clinical validation cohorts of non-dialysis dependent CKD and dialysis-dependent ESRD patients with VC measurements

We prospectively enrolled two cohorts of patients; one with dialysis-dependent ESRD for experimental finding validation and the other with non-dialysis dependent CKD for independent validation. The procedure for cohort establishment is detailed in the supplemental method. The study protocol was approved by the institutional review board of the National Taiwan University Hospital (NO. 201208069RIC, NO. 201508045RINA, and NO. 201710041RIND), and adhered to the Declaration of Helsinki. Informed consent has been obtained from all participants. Quantitation of circulating miRNAs and proteins of interest was done based on strategies outlined in the supplemental method. For VC phenotype determination, we gauged participants' aortic arch calcification (AAC) based on their posteroanterior chest radiography collected on enrollment. Semi-quantitation of AAC was accomplished based on previously validated radiologic criteria; briefly, those without calcification, with trace/spotty calcified lesions, with linear/semilunar shaped calcified lesion, and with near circumferential lesion were assigned stage 0, 1, 2, and 3 VC,

respectively.[15,22] AAC severity exhibits a close relationship with calcification extent over the entire aorta and with the risk of cardiovascular events, as shown in the existing literature.[23,24]

2.13 Statistical analysis

The statistical approaches for analyzing clinical data in the CKD and ESRD cohort are described in the supplemental method.

3. RESULTS

3.1 Testing and optimizing the 3-tiered in vitro *model of uremic VC*

The components of the 3-tier uremic VC models are described in Figure 1A. After 10 days of HP exposure, aortic VSMCs exhibited progressively increasing calcification, from control, HP, to HP+T, HP+D, and HP+I groups both macroscopically and microscopically (Figures 1B and 1C). We next determined the dose-response and time-response relationships between aggravating factors (TNF-α, VitD, and IS) (Figure 1A) and calcification severity to select optimal conditions for collecting microarray samples. A time-dependent increase in calcification was observed in VSMCs exposed to HP+D at all tested doses at 7 and 10 days, while only the 10 nM VitD group exhibited significantly higher calcification than the HP alone group at 10 days of exposure (Figure S1A). Similar time-dependent increases in

calcification were found in HP+T and HP+I treated VSMCs at all doses, and only 10 ng/mL TNF-α (Figure S1B) and 250 μM IS (Figure S1C) induced significantly greater calcification severity than the other doses of TNF-α and IS at 10 days, respectively. We further showed that the co-administration of the selected doses of TNF-α, VitD, and IS to HP-treated VSMCs resulted in a stepwise elevation of *RUNX2* expressions in treated VSMCs compared to HP only and non-calcified ones (Figure 1D).

3.2 Animal model of uremic VC

Rats receiving adenine (CKD group) and adenine+HP (CKD+HP group) diet had progressive decline in body weight over 12 weeks, while those on normal chow (control group) gained weight (Figure 1E). CKD and CKD+HP group rats had 5- to 6-fold increases in serum creatinine (Figure 1F), accompanied by histopathological evidence of tubular dilatation, epithelial flattening, and interstitial fibrosis on Masson trichrome staining (Figure 1G). In the control, CKD, and CKD+HP groups, the total kidney injury scores were 0, 16.7 ± 1.6, and 17.3 ± 1, respectively, compatible with the trend in serum creatinine levels (Figure 1F). Progressively greater aortic medial calcification was noted from control, CKD to CKD+HP group (Figure 1H), and quantification of aortic calcification areas showed the same findings (Figure 1I). VC severities did not correlate with total kidney injury scores in CKD group (r = 0.72, p = 0.11), while a positive correlation was observed in CKD+HP group (r = 0.86, p =

0.03). VC severities correlated significantly with the scores of interstitial inflammations in CKD+HP group (r = 0.91, p = 0.01) but not in CKD group (r = -0.01, p = 0.99). In addition, VC severities exhibited a trend of positive correlation with the scores of tubular dilatations with epithelial flattening (r = 0.79, p = 0.06) in CKD+HP group but not in CKD group (r = 0.72, p = 0.11). CKD+HP group rats had significantly lower serum calcium and higher serum phosphate than those of the CKD group (Figure 1J), while aortic *RUNX2* and osteocalcin expression was significantly elevated in the CKD+HP and CKD, CKD+HP groups, respectively (Figure 1K). These findings support the validity of our uremic VC animal models.

3.3 Microarray and bioinformatic-assisted uncovering of differentially expressed miRNAs/genes

A detailed algorithm for screening target miRNAs and genes is provided in Figure 2. Briefly, VSMCs treated with DMEM, HP, HP+D, HP+T, and HP+I at pre-selected concentrations, as well as aortic media from control, CKD, and CKD+HP rats, were harvested and sent for miRNA and mRNA microarray analyses. Heatmaps for all tested miRNAs and genes in cells and tissues are shown in Figures 3A and 3B. All tested miRNAs underwent correlation testing between cell and tissue samples, and those which were significant were further screened for stepwise divergences from control groups, as shown in scatter plots of paired

comparisons of each condition (Figure 3C). In total 122 down-regulated and 119 up-regulated miRNAs during the course of increasing calcification were identified initially (Figure 2, with *p* values of each miRNA shown in the Table S2). These DEMis were further filtered based on prediction databases, assisted by findings from mRNA microarray assays, followed by selection based on the directional criterion (anti-correlations). At this step, 112 deregulated miRNAs and 140 pairing genes were discovered (up-regulated miRNAs with down-regulated genes, Figure 3D; down-regulated miRNAs with up-regulated genes, Figure 3E). Targets of the negatively deregulated miRNAs frequently belonged to BPs related to muscle or bone tissues (5 out of 44 GO terms, which contain >1 mRNA targets per GO term), while the targets of the positively deregulated miRNAs did not have any BP related to the bone, muscle, and vascular tissues identified (0 out of 128 GO terms) (Table S3). Further gene annotation and functional enrichment of filtered gene results showed that ossification process was the most prominently altered biological pathway, followed by extracellular matrix organization, osteoblast differentiation, and vessel morphogenesis (Figure 3F). In addition, totally 279 enriched BPs of the associated networks based on the BIOGRID PPI database (adjusted *p*-value < 0.01) (Table S4) and 918 enriched BPs based on the STRING PPI database (Table S5) were retrieved. We proceeded with BIOGRID-derived results since BIOGRID has higher yield-coverage for experimentally verified interactions and less redundant predicted interactions compared to those from STRING. Sixteen DEMis (9

down-regulated and 7 up-regulated) and 14 of their predicted targets stood out as potentially important biomarker candidates based on the annotation results. Heatmaps for the 16 DEMis and 14 potential gene targets are shown in Figures 3G and 3H, respectively. Further evaluation by KEGG and GO-assisted networks of BP-associated gene clusters based on down-regulated (Figure 3I) and up-regulated DEMis (Figure S1D) are shown. Molecules pertaining to muscle, bone, immunity, and vessel physiology constitute a major proportion of these gene clusters. Up-regulated DEMis had significantly fewer associated genes compared to down-regulated ones (Figure S1D). After taking gene expression levels into consideration, we found that only down-regulated DEMis (n = 9) had their target gene expression with a matching trend of changes during progressive calcification, while up-regulated DEMis (n = 7) did not have corresponding target genes identified.

3.4 Validation of miRNA and mRNA expressions in in vitro *rat VSMCs and* in vivo *rat aortic samples*

To ascertain expression results for the established models, we performed qPCR for identified DEMis and gene candidates in calcified VSMC samples. Among 9 down-regulated DEMis, only 5 (miR-10b-5p, 125b-2-3p, 195, 378a-3p, and 592) exhibited a trend of decline in expression over at least one aggravating calcification model (Figure 4A), while the other 4 DEMis did not (Figure S2A). Nearly all up-regulated DEMis during calcification progression

failed to exhibit a compatible trend (Figure S2B; one was not assayed for absence of validated primer). Validation of the 14 candidate genes in the *in vitro* model showed that 7 genes were up-regulated, paralleling higher calcification severity and the opposite changes of their paired miRNAs (Figure 4A), while the other 7 did not (Figure S2A). To exclude the possibility of systemic errors, we examined the expressions of another two un-selected up-regulated DEMis during calcification and compared their *in vitro* expression levels with those in the array (Figure S2C), with consistent result alignment shown. The coherence between our *in vitro* validation findings and microarray data was therefore good.

We also analyzed the correlation between the expression levels of the 5 *in vitro* validated miRNA (miR-10b-5p, 195, 125b-2-3p, 378a-3p, and 592) and between the 5 miRNAs and RUNX2 mRNA levels (Figure S2D). We found that miR-195 expressions poorly correlated with those of the other 4 miRNAs except miR-592, while miR-378a-3p and 10b-5p exhibited closer correlations with the other miRNAs. The expression levels of RUNX2 mRNA correlated more closely with miR-195 and 592 compared with the other 3 miRNAs (Figure S2D).

When validated *in vivo*, only 4 DEMis (miR-10b-5p, 125b-2-3p, 195, and 378a-3p) exhibiting progressive down-regulation during greater aortic calcification (Figures 4B and

S3A), while the other 5 did not (Figure S3B). Among the 14 candidate mRNA, only 2 (*SULF1* and *MYOZ2*) demonstrated up-regulation during aortic calcification (Figures 4B and S3A), while the other 12 did not (Figure S3B). Similar to the *in vitro* findings, none of the up-regulated DEMis was validated *in vivo* (Figure S3C). Based on the above *in vitro* and *in vivo* results, 4 DEMis and 2 genes were chosen to enter the subsequent step of biomarker test; miR-378a-3p was predicted *in silico* to regulate *SULF1*, while *MYOZ2* was predicted to be a target of miR-592, not included in the 4 selected DEMis.

3.5 Expression level validation in the ex vivo model

In the *ex vivo* model, rat aortas exhibited prominent circumferential calcification upon HP treatment (Figure S4A). The 4 DEMis were similarly down-regulated during aortic calcification (Figure 4C and Figure S4B), while only *SULF1* was up-regulated in terms of both mRNA expression and protein levels (Figure 4C) whereas *MYOZ2* was not (Figure S4B). This was accompanied by 1.6- and 5-fold higher expression of aortic *RUNX2* and *ALP*, respectively (Figure S4C).

3.6 Expression level validation in calcified human ASMCs

We further examined whether the expression levels of these 4 DEMis and SULF1 exhibited the same trend in two types of human ASMCs during calcification. Prominent calcification

was observed in SI-354 cells exposed to HP medium grossly and microscopically (Figure S4D). The 4 DEMis declined significantly under HP treatment in both PCS-100 and SI-354 cells, with a greater degree of decline paralleling higher medium phosphate concentrations (Figure S4E, left). Finally, lower DEMis expressions were accompanied by an increase in SULF1 expression levels in both human ASMCs (Figure S4E, right).

3.7 Functional characterization of the 4 DEMis and their target mRNA in VSMCs

Aortic VSMCs were transfected with each of the 4 DEMi mimics and treated with HP to assess whether these miRNAs regulated VC. At baseline, there was no difference in calcium deposition amount without HP exposure between each group. After successful DEMi transfection (Figure S5A), we first checked whether cell proliferation and contractility were altered. Overexpression of the 4 DEMis did not modulate VSMC proliferative ability (Figure S5B) nor their contractility (Figures S5C and S5D). Following HP exposure, miR-10b-5p, 125b-2-3p, and 378a-3p overexpressing VSMCs had significantly less microscopic and macroscopic calcification nodules compared to control or scrambled miRNA transfected ones, while miR-195-5p overexpressing VSMCs did not (Figure 4D). VSMCs overexpressing miR-10b-5p, 125b-2-3p, and 378a-3p had approximately 20%, 28%, and 22% lower calcium deposition than controls (Figure 4E, left upper). Compared to non-HP treated VSMCs, miR-10b overexpressing cells treated with HP exhibited significantly lower osteocalcin

(Figure 4E, left lower) and *SULF1* (Figure 4E, right lower) expression than scrambled controls, while HP-treated miR-125b-2-3p overexpressing VSMCs had significantly suppressed alkaline phosphatase (Figure 4E, right upper) and *SULF1* (Figure 4E, right lower) levels compared to scrambled controls. HP-treated miR-378a-3p overexpressing VSMCs had significantly lower osteocalcin, alkaline phosphatase and *SULF1* levels compared to HP-treated controls (Figure 4E).

We further silenced *SULF1* expressions in VSMCs to observe whether *SULF1* participated in the pathogenesis of VC. HP induced more severe calcification in all controls and mock siRNA groups, but calcification was ameliorated in *SULF1*-silenced group (Figure 4F). Following HP exposure, control VSMCs exhibited a significant increase in *SULF1* expressions, while siRNA-transfected VSMCs had significantly lower *SULF1* expressions (Figure 4G, upper) accompanied by lower calcium depositions compared to controls (Figure 4G, lower), supporting its functional role in VC pathogenesis.

3.8 Verification of direct binding of DEMi to the 3'-UTR of their predicted target

Dual-luciferase reporter assays were performed to confirm the existence of the predicted miR-378a-3p/*SULF1* pair (Figure 4H, upper). After co-transfecting cells with miR-378a-3p mimics and luciferase plasmids with *SULF1* 3'-UTR sequences or the seed region, we found

that luciferase activities of both groups significantly decreased compared to those of controls (Figure 4H, lower). When the seed region was mutated, the luciferase activities recovered completely (Figure 4H, lower).

3.9 Exploring the plausibility of DEMis as potential biomarkers for uremic VC

We discovered that the expression levels of the 4 candidate DEMis declined upon calcification concurrently within cells and the culture media *in vitro* (Figure 5A). The expression levels of the 4 DEMis exhibited the same trend within calcified aortas and the culture media *ex vivo* (Figure 5B). This was also observed in the cultured media of HP-treated human ASMCs regarding the expressions of miR-125b-2-3p, 195, and 378a-3p, except 10b-5p (Figure 5C). Furthermore, the circulating levels of the 4 DEMis exhibited compatible trends of decline accompanying greater aortic calcification (Figure 5D). These findings imply that these 4 DEMis might be potential candidate biomarkers for indicating uremic VC presence and its severity. We thus focused on the 4 miRNAs and *SULF1* as potential miRNA- and target protein-based marker pair for predicting uremic VC in subsequent experiments.

3.10 Clinical utility of the DEMis and target genes as circulating biomarkers for uremic VC

From two institutes, we prospectively enrolled 96 ESRD patients, among whom 28 (29.2%) did not have VC, while 68 (70.8%) had AAC of different severities. Among those with AAC, 34 (50%), 24 (35.3%) and 10 (14.7%) had stage 1, 2 and 3 VC, respectively (Table 1). Part of the ESRD patients (n = 19) without VC had incomplete clinical features upon recruitment (such as physical parameters), and their data were excluded during the subsequent regression analyses. Clinical features from excluded patients did not differ significantly from those of the remaining participants. Patients with greater VC severity had significantly more advanced ages and more likely to have diabetes and received clopidogrel compared to those without or with milder VC (Table 1).

We subsequently examined the distribution of circulating *SULF1* and miRNAs among the ESRD cohort (n = 96). Circulating *SULF1* (3.63 [0.47, 7.82] ng/mL), miR-10b-5p (1.11 [0.54, 11.19]), miR-195 (16.8 [3.27, 63.61]), miR-125b-2-3p (3.49 [0.89, 20.94]), and miR-378a-3p (0.83 [0.31, 4.2]) levels were non-normally distributed (all Kolmogorov-Smirnov p <0.001). Those with uremic VC had significantly lower circulating miR-125b-2-3p (with vs. without, 1.87 [0.6, 8.13] vs. 27.03 [15.44, 59.76]; p <0.001) and miR-378a-3p (0.52 [0.23, 1.5] vs. 10.77 [3.08, 32.06]; p <0.001) levels than those without (Figure 6A), while there were no differences regarding circulating miR-10b-5p (with vs. without, 1.23 [0.42, 21.95] vs. 0.91 [0.62, 4.67]; p = 0.821) and miR-195 (21.87 [4.87, 102.22] vs. 3.51 [0.55, 33.4]; p = 0.056)

levels (Figure S6A). Patients with greater VC severity also had progressively lower circulating miR-125b-2-3p and 378a-3p levels (Figure 6B), while miR-10b-5p and 195 levels did not (Figure S6B). Furthermore, circulating *SULF1* levels were significantly higher among those with uremic VC than those without (5.81 [2.8, 10.7] vs. 0.2 [0.19, 0.53] ng/mL, p <0.001), and *SULF1* levels rose successively with increasing VC severity (Figure 6C). In addition, we found that the 3 significant biomarkers (*SULF1*, miR-378a-3p, and miR-125b-3p) tightly correlated with each other (for *SULF1* vs. miR-378a-3p, r = -0.35, p <0.001; for *SULF1* vs. miR-125b-2-3p, r = -0.44, p <0.001; for miR-125b-2-3p vs. miR-378a-3p, r = 0.41, p <0.001). We did not identify any sex-specific differences in *SULF1* or in the 4 miRNA levels (male vs. female, for circulating *SULF1*, miR-10b-5p, 195, 378a-3p, and 125b-2-3p levels, p = 0.473, 0.478, 0.285, 0.804, and 0.274, respectively).

Multiple logistic regression with VC presence as the dependent variable (n = 77) showed that conventional clinical variables, including age, gender, diabetes, and clopidogrel use, failed to exhibit independent associations with VC (model 1; Table 2). After adding *SULF1* levels into the regression model, we found that higher circulating *SULF1* was independently associated with an increased probability of VC (odds ratio [OR] 1.419, 95% confidence interval [CI] 1.044 – 1.928) (model 2; Table 2). Adding miR-125b-2-3p or miR-378a-3p into the clinical variable-only model showed that miR-125b-2-3p (OR 0.939, 95% CI 0.896 – 0.984) or

miR-378a-3p (OR 0.854, 95% CI 0.769 – 0.949) exhibited an independently negative relationship with VC in ESRD patients (models 3 and 4; Table 2). If we accounted for *SULF1*, miR-125b-2-3p and miR-378a-3p together, only miR-378a-3p and *SULF1* were independent factors associated with uremic VC (model 5; Table 2), while miR-125b-2-3p was not. The performance of regression models predicting VC probability increased stepwise when we considered miR-125b-2-3p only, *SULF1* only, miR-378a-3p only, or all three biomarkers together (AUROC for clinical, clinical+miR-125b-2-3p, clinical+*SULF1*, clinical+miR-378a-3p, and clinical+*SULF1*+both miRNAs; 0.5, 0.732, 0.792, 0.85, and 0.923, respectively) (Figure 6D). Similar findings were obtained when we plotted results of the 5 models using the precision-recall curves (Figure 6E). We also examined whether age and gender modified the relationship between *SULF1*, the 2 miRNAs, and VC probability (Table S6). Age and gender failed to influence the relationship between circulating miRNA and VC risk.

We undertook sensitivity analyses to reassure the validity of our findings. An ordinal regression analysis with different VC categories as the dependent variable, incorporating the same set of variables as in model 5 of Table 2, showed that miR-378a-3p (OR 0.872, 95% CI 0.763 – 0.973) remained negatively associated with VC, while SULF1 (OR 1.287, 95% CI

1.167 – 1.447) was positively associated. On the other hand, circulating miR-125b-2-3p was insignificant for predicting VC probability (p = 0.422) (Table S7).

3.11 Validation of the DEMis and their target gene as biomarkers in patients with CKD

We further validated our findings in another cohort of 59 non-dialysis dependent CKD patients (mean 73 ± 11 years; 66.1% male), among whom 32 (54.2%) were diabetic and 36 (61%) had uremic VC. Similarly, those with uremic VC had significantly lower circulating miR-125b-2-3p (with vs. without, 1.21 [0.51, 1.93] vs. 6.67 [4.51, 9.36]; p < 0.001) and miR-378a-3p (0.11 [0.06, 0.16] vs. 0.67 [0.56, 0.95]; p < 0.001) levels than those without (Figure 6F), while there were no differences regarding miR-10b-5p (with vs. without, 1.05 [0.72, 2.14] vs. 1.31 [0.55, 4.84]; p = 0.111) and miR-195 (1.68 [0.78, 3.56] vs. 3.29 [1.65, 7.46]; p = 0.371) levels (Figure S6C). Patients with a greater VC severity also had progressively lower circulating miR-125b-2-3p and 378a-3p levels (Figure 6G), while miR-10b-5p and 195 levels did not (Figure S6D). Furthermore, circulating *SULF1* levels were significantly higher among those with uremic VC than those without (2.14 [0.61, 2.63] vs. 0.2 [0.195, 0.46] ng/mL, p < 0.001), and rose successively with increasing VC severity (Figure 6H). Regression analyses showed that circulating miR-125b-2-3p (OR 0.042, 95% CI 0.003 – 0.547) and miR-378a-3p (OR 0.009 95% CI < 0.001 – 0.004) were both negatively

associated with VC, while SULF1 (OR 6.263, 95% CI 1.922 – 20.412) was positively associated.

4. DISCUSSION

In this translational study, HP-treated VSMCs and animal aortas with uremic VC were subjected to miRNA and transcriptomic profiling. We selected miRNAs and mRNAs exhibiting expression level changes paralleling the severity of the VC phenotype, and validated the changes to these candidate biomarkers in multiple cellular and animal models. We further demonstrated that some of the selected miRNAs and their target mRNA exhibited functional influences on VC. Finally, we discovered that serum miR-378a-3p in combination with their pair gene *SULF1*, in sera of non-dialysis CKD and dialysis-dependent ESRD patients were independently associated with uremic VC and the extent of VC severity with better performance than that shown by clinical features alone or with target protein only. Finally, the miRNA-target gene pair functionally regulates the pathologic process of VC and serves potentially as therapeutic targets. We believe that our findings represent a significant leap forward in the quest to identify uremic patients at an increased risk of developing VC, using molecular regulation-based (miRNA-mRNA) paired biomarkers (Figure 6I).

It is observed that the expression of candidate miRNAs did not behave consistently among the 3 escalating calcification models (Figure 4A). We believe that this is not unexpected. For the 5 miRNAs we validated *in vitro*, there are evidence supporting a modification effect on miRNA expressions related to the escalating stimuli we administered. Prior studies identified that TNF-α could induce miR-10b expression through activating NF-kB[25]; it is plausible that although TNF-α aggravates VC, it may up-regulate certain miRNAs concurrently. Similarly, 1,25-dihydroxy-vitamin D has been shown to up-regulate hypoxia-inducible factor (HIF)-1α in the vascular wall, while HIF-1α increases miR-10b expressions.[26,27] It is possible that the down-regulation of miR-10b in the HP model is partially attenuated in the HP+D model (Figure 4A). Along this line, miR-592 expression in several cell types has also been found to be affected by adipokines, inflammation, and metabolic disorders.[28,29] The addition of TNF-α may alter the expression of miR-592 in our HP+T model as well (Figure 4A). Consequently, the trend of miRNA changes may not be homogeneous across the escalating calcification models we utilized in this study.

In the *in vivo* model, we found that serum phosphate levels and aortic RUNX2 expression did not differ between the control and the CKD group (Figure 1K). Several reasons may be responsible for this finding. Existing literature suggests that the murine model of adenine-induced CKD alone may not necessarily harbor VC, which is more dependent on

dietary phosphate content. Tani *et al* showed that animals receiving adenine-containing diet supplemented with high phosphate had uniformly prominent aortic calcification, while those receiving adenine-containing diet with normal phosphate only had mild numerically higher aortic calcium content without significant differences compared to controls receiving standard chows.[30] What seems to be a more important contributor to the development of aortic calcification in this model is the degree of serum phosphate elevation. Tani *et al* showed that mice receiving adenine/high phosphate diet had substantially higher (160-180%) serum phosphate levels than those in controls, accompanied by a prominently increased VC in the former group. Similarly, Terai *et al*. discovered in an adenine model that adenine diet alone induced VC in less than 50% rats.[31] In our previous work[15], we similarly found that serum phosphate levels and aortic RUNX2 expressions failed to reach difference between the control and the adenine group, with a wide confidence interval in the latter group, similar to the present findings. The amount of food intake among animals can be another potential reason. A prior review described that 0.75% dietary adenine concentration used in our model led to rapid kidney damages, decreased oral intake, and weight loss.[32] Since dietary phosphate is an integral determinant of serum phosphate levels in individuals with CKD[33], it is likely that some of the CKD rats with worsening renal function ingest less chow than the control group, leading to relatively low serum phosphate levels at the end of experiments.

The concept of using miRNA-mRNA pairs as a circulating biomarker panel to diagnose disease is rarely tested, and has substantial clinical applicability. Existing studies seeking genetic marker-based disease recognition mostly involve single nucleotide polymorphisms (SNPs) or miRNAs alone or in combination, with and without subgroup categorization or differential component weighting.[15,34] However, SNP-based markers often correlate with susceptibility to disease development, but less frequently with disease severity, and are affected by obscuring outliers. The use of circulating miRNAs as biomarkers may obviate part of these shortcomings, as different cell types have been shown to secrete specific miRNAs into the extracellular space and biologic fluids including sera. Despite their advantage as a non-invasive biomarker using liquid biopsy and their good diagnostic good sensitivity and specificity, single miRNAs frequently fail to capture subtypes within one disease, and expression differences between cases and controls may not be large enough.[35] The emerging trend for circulating miRNA-based diagnostics then turns to miRNAs in combination or miRNAs combining other clinical indicators for optimizing biologic phenotype characterization.[35] Recent studies support this notion by showing that miRNA panels or miRNA-methylation marker combinations could successfully differentiate between diseased and non-diseased status.[36,37] However, using miRNA and their target genes as combinatorial biomarkers is a under-recognized approach, despite the advantage of potentially higher specificity than each marker alone. Using miRNA-mRNA expression

database and network analysis, Tian *et al*. showed that miR-423-5p and *v-Myc* pair could predict the presence of nasopharyngeal carcinoma with reasonable performance.[38] This approach has not been tested for its applicability in vascular pathologies. As a first attempt, we devised a translational study by screening for potential miRNA and mRNA biomarkers in different calcification severity models, followed by extensive experimental validation and finally in clinical specimens. Moreover, the performance of regression models gauging VC probability substantially and progressively increased with the addition of miRNA and their target protein levels (Figure 6D). Consequently, our results suggested that miRNA-mRNA pairs as biomarkers is feasible in distinguishing uremic patients with and without VC, creating a new and specific approach for recognizing those at greater risk of developing or having worse VC.

Three new biomarkers were identified in this study, miR-125b-2-3p, miR-378a-3p, and *SULF1*. *SULF1* encodes heparan sulfatase 1, which is widely expressed in tissues and potentially modulates Wnt, fibroblast growth factor (FGF), and bone morphogenetic protein (BMP) pathways through re-shaping proteoglycan in extracellular matrix.[39] According to the human protein atlas, the organ with the highest expression of *SULF1* is smooth muscles including vascular tissues.[40] *SULF1* also plays an important role in VSMC physiology; over-expression of *SULF1* in VSMCs has been reported to impair their adhesion ability, with

increased apoptosis, migration, and chemotaxis.[41] Furthermore, *SULF1* enhances Wnt signaling in vascular tissue[42], while the activation of Wnt/β-catenin pathways promotes the development of VC.[43] The up-regulation of *SULF1* may theoretically participate in the course of uremic VC, although existing studies have not directly addressed this possibility. Another plausible mechanism involves the SULF1-associated modulation of angiotensin II receptor expressions in VSMCs, which reportedly promotes osteogenic differentiation.[44,45] Judging from their direct targeting relationship and their known participation in vascular physiology, we propose that miR-378a-3p could exert regulatory influences on *SULF1* expression in VSMCs during VC.

From *in silico* analysis, we were able to identify several downstream miR-125b-2-3p targets that are potentially involved in osteoblastic differentiation or phosphate homeostasis such as *CTNNBIP1*, *UCHL1*, and *SIRT1*, all of which have been shown to participate in the pathogenesis of VC.[46,47] On the other hand, miR-378a-3p exhibits pleiotropic effects on angiogenesis, muscle cell proliferation and differentiation by promoting myogenesis, myocyte survival, and inhibiting apoptosis. Based on an online miRNA expression database, *miRmine* (http://guanlab.ccmb.med.umich.edu/mirmine), vascular tissues exhibit high expression levels of miR-378a-3p compared to the other organs. MiR-378a-3p also has multiple *in silico* targets that presumably play a role in bone development and calcification

development, including BMP2 and ERK2. An increased BMP2 expression is frequently found in calcified atheroma and suppressing BMP2 levels can attenuate VC severity.[48] VSMC osteoblastic trans-differentiation also involves the activation of ERK1/2, and molecules inhibiting ERK1/2 expressions similarly ameliorate VC.[49] Another plausible target of miR-378a-3p, Ca^{2+}/calmodulin-dependent protein kinase II (CAMKK2), has been reported to promote stem cell differentiation toward the osteoblastic lineage.[50] These mRNA targets, in combination with miR-125b-2-3p and miR-378a-3p, may all participate in the pathogenic picture of uremic VC.

In Figures 4E and 4F, HP-treated VSMCs with miR-10b-5p, 378a-3p, and 125b-2-3p over-expression exhibited significantly less calcification compared with the controls but differences in osteocalcin expression were not evident in the miR-125b-2-3p over-expression cells (Figure 4E). This phenomenon may be explained by several reasons: first, the confidence interval of osteocalcin expression in the negative control group was relatively wide. Second, osteocalcin is one of the downstream effectors of RUNX2, and the degree of the downplay of signals related to osteoblast-like activity may differ between early effectors such as RUNX2 and late effectors such as osteocalcin. Nonetheless, the trend of changes of osteocalcin expressions in the miR-125b-2-3p over-expression group is still compatible with changes in calcium depositions of the same group (Figure 4E).

Several limitations need to be considered before interpreting our results. Although we used multiple experimental models to screen for and validate our candidate biomarkers, it is still possible that our approach did not capture the entire etiological spectrum of uremic VC, reducing the probability of identifying more markers. The miRNA and mRNA microarray experiments we performed were cross-sectional in nature, and the trend of changes in miRNA and mRNA expression might differ depending on the temporal course of VC. Our strict selection strategy also constituted a barrier against uncovering more broadly defined biomarkers. As explained above, serum phosphate and aortic RUNX2 did not differ between the control and the CKD rats; however, we have reassured the reliability of our in vivo model through examining aortic osteocalcin expressions, which were significantly stronger in the CKD group than those in the control group (Figure 1K). Aortic rings from the CKD group also showed prominent von Kossa positive staining and significantly higher quantitative staining areas compared to those from the control group (Figure 1H). The degree of atherosclerotic VC and the use of anti-platelet agents might influence our findings, although we have adjusted for these factors in the clinical analysis. In addition, it remains unclear whether our findings are applicable to those of other ethnic groups, such as Caucasians or African-Americans. Validation of our results in different cohorts or populations may be

needed. Finally, the therapeutic role of the miRNA-target pair we identified in uremic VC has not been explored in depth.

CONCLUSIONS

In summary, we used miRNA and transcriptomic profiling to screen for and identify potential miRNA and mRNA candidate biomarkers for uremic VC. Through serial validation in *in vitro*, *in vivo*, and *ex vivo* models, we discovered that miR-10b-5p, miR-195, miR-125b-2-3p, miR-378a-3p and its target *SULF1* may be potential biomarkers, while the list was further narrowed to miR-378a-3p and *SULF1* after evaluation in sera from CKD and ESRD patients. The inclusion of these miRNA/protein biomarkers for gauging the probability of uremic VC, in addition to clinical features, could prominently improve how we diagnose uremic VC. We believe that a combined biomarker panel, including miRNAs and their target proteins, may represent a potentially useful approach in recognizing ESRD patients prone to developing VC or who could be subjected to worsening VC.

ACKNOWLEDGEMENTS

We are grateful to all the staffs and assistants of the National Taiwan University Genomic Center and the second core laboratory, Department of Medical Research of National Taiwan University Hospital for cell experiments and sample preparations. The abstract of this study

has been accepted for ePoster presentation in the Annual meeting of the American Society of Nephrology (Kidney Week 2020).

Funding disclosure: The work was supported by the Ministry of Science and Technology, Taiwan [MOST-108-2314-B-002-055-, MOST-108-2321-B-038-003-, and MOST-109-2314-B-002-193-MY3]. The sponsor has no role in the performance, data analysis and interpretation of the study results.

Conflict of interest disclosure: The authors have no relevant competing interests to declare in relation to this manuscript.

Author contribution

CTC, HYY, and HWC are responsible for conception and design of this study; CTC, YTT, and HYY are responsible for acquisition of data; CTC, YTT, and HYY are responsible for analysis and data interpretation; CTC, YTT, HYY, CKC, and HWC drafted and revised the manuscript; all authors read the manuscript and approved the submission of this manuscript.

Data availability statement

The experimental part of data underlying this article are available in the article and its online supplemental materials. The clinical part of data will be shared on reasonable request to the corresponding author.

Reference

1. Wang X-R, Zhang J-J, Xu X-X, Wu Y-G. Prevalence of coronary artery calcification and its association with mortality, cardiovascular events in patients with chronic kidney disease: a systematic review and meta-analysis. *Renal Fail* 2019;**41**:244-256.
2. Jono S, Shioi A, Ikari Y, Nishizawa Y. Vascular calcification in chronic kidney disease. *J Bone Miner Metab* 2006;**24**:176-181.
3. Kakani E, Elyamny M, Ayach T, El-Husseini A. Pathogenesis and management of vascular calcification in CKD and dialysis patients. *Semin Dial* 2019;**32**:553-561.
4. Niu Q, Hong Y, Lee C-H, Men C, Zhao H, Zuo L. Abdominal aortic calcification can predict all-cause mortality and CV events in dialysis patients: A systematic review and meta-analysis. *PLOS ONE* 2018;**13**:e0204526.
5. Chen S-C, Teh M, Huang J-C, Wu P-Y, Chen C-Y, Tsai Y-C, Chiu Y-W, Chang J-M, Chen H-C. Increased Aortic Arch Calcification and Cardiomegaly is Associated with Rapid Renal Progression and Increased Cardiovascular Mortality in Chronic Kidney Disease. *Sci Rep* 2019;**9**:5354.
6. Ruospo M, Palmer SC, Natale P, Craig JC, Ve cchio M, Elder GJ, Strippoli GF. Phosphate binders for preventing and treating chronic kidney disease-mineral and bone disorder (CKD-MBD). *Cochrane Database Syst Rev* 2018;**8**:CD006023.
7. Nicoll R, Henein M. Arterial calcification: A new perspective? *Int J Cardiol* 2017;**228**:11-22.
8. Moe Sharon M, Chen Neal X. Pathophysiology of Vascular Calcification in Chronic Kidney Disease. *Circ Res* 2004;**95**:560-567.
9. Ruderman I, Holt SG, Hewitson TD, Smith ER, Toussaint ND. Current and potential therapeutic strategies for the management of vascular calcification in patients with chronic kidney disease including those on dialysis. *Semin Dial* 2018;**31**:487-499.
10. Gross P, Six I, Kamel S, Massy ZA. Vascular Toxicity of Phosphate in Chronic Kidney Disease – Beyond Vascular Calcification –. *Circ J* 2014;**78**:2339-2346.
11. Metzinger-Le Meuth V, Burtey S, Maitrias P, Massy ZA, Metzinger L. microRNAs in the pathophysiology of CKD-MBD: Biomarkers and innovative drugs. *Biochim Biophys Acta Mol Basis Dis* 2017;**1863**:337-345.
12. Harrill AH, McCullough SD, Wood CE, Kahle JJ, Chorley BN. MicroRNA Biomarkers of Toxicity in Biological Matrices. *Toxicol Sci* 2016;**152**:264-272.
13. Zhang Y, Zhang L, Wang Y, Ding H, Xue S, Qi H, Li P. MicroRNAs or Long Noncoding RNAs in Diagnosis and Prognosis of Coronary Artery Disease. *Aging Dis* 2019;**10**:353-366.
14. Fung EC, Butt AN, Eastwood J, Swaminathan R, Sodi R. Chapter Three - Circulating microRNA in cardiovascular disease. In: Makowski GS, editor. Advances in Clinical Chemistry. 91: Elsevier; 2019. p. 99-122.

15. Chao C-T, Liu Y-P, Su S-F, Yeh H-Y, Chen H-Y, Lee P-J, Chen W-J, Lee Y-M, Huang J-W, Chiang C-K, Hung K-Y, Chen HW. Circulating MicroRNA-125b Predicts the Presence and Progression of Uremic Vascular Calcification. *Arterioscler Thromb Vasc Biol* 2017;**37**:1402-1414.

16. Madhavan B, Yue S, Galli U, Rana S, Gross W, Müller M, Giese NA, Kalthoff H, Becker T, Buchler MW, Zoller M. Combined evaluation of a panel of protein and miRNA serum-exosome biomarkers for pancreatic cancer diagnosis increases sensitivity and specificity. *Int J Cancer* 2015;**136**:2616-2627.

17. Shackelford C, Long G, Wolf J, Okerberg C, Herbert R. Qualitative and quantitative analysis of nonneoplastic lesions in toxicology studies. *Toxicol Pathol* 2002;**30**:93-96

18. Maric C, Sandberg K, Hinojosa-Laborde C. Glomerulosclerosis and tubulointerstitial fibrosis are attenuated with 17β-Estradiol in the Aging Dahl salt sensitive rat. *J Am Soc Nephrol* 2004;**15**:1546-1556

19. Canales BK, Reyes L, Reinhard MK, Khan SR, Goncalves CG, Meguid MM. Renal glomerular and tubular injury after gastric bypass in obese rats. *Nutrition* 2012;**28**:76-80

20. McNemar Q. Note on the sampling error of the difference between correlated proportions or percentages. *Psychometrika* 1947;**12**:153-157.

21. Bilder CR, Loughin TM. Testing for Marginal Independence between Two Categorical Variables with Multiple Responses. *Biometrics* 2004;**60**:241-248.

22. Chao CT, Yuan TH, Yeh HY, Chen HY, Huang JW, Chen HW. Risk Factors Associated With Altered Circulating MicroRNA-125b and Their Influences on Uremic Vascular Calcification Among Patients With End-Stage Renal Disease. *J Am Heart Assoc* 2019;**8**:e010805.

23. Li J, Galvin HK, Johnson SC, Langston CS, Sclamberg J, Preston CA. Aortic Calcification on Plain Chest Radiography Increases Risk for Coronary Artery Disease. *Chest* 2002;**121**:1468-1471.

24. Hashimoto H, Iijima K, Hashimoto M, Son B-K, Ota H, Ogawa S, Eto M, Akishita M, Ouchi Y. Validity and Usefulness of Aortic Arch Calcification in Chest X-Ray. *J Atheroscler Thromb* 2009;**16**:256-264.

25. Li X, Gao L, Cui Q, Gary BD, Dyess DL, Taylor W, Shevde LA, Samant RS, Dean-Colomb W, Piazza GA, Xi Y. Sulindac inhibits tumor cell invasion by suppressing NF-kB mediated transcription of microRNAs. *Oncogene* 2012;**31**:4979-4986.

26. Wong MS, Leisegang MS, Kruse C, Vogel J, Schumann C, Dehne N, Weigert A, herrmann E, Brune B, Shah AM, Steinhilber D, Offermanns S, Carmeliet G, Badenhoop K, Schroder K, Brandes RP. Vitamin D promotes vascular regeneration. *Circulation* 2014;**130**:976-986.

27. Haque I, Banerjee S, Mehta S, De A, Majumder M, Mayo MS, Kambhampati S, Campbell DR, Banerjee SK. Cysteine-rich 61-connective tissue growth factor-nephroblastoma-overexpressed 5 (CCN5)/Wnt-1-induced signaling protein-2 (WISP-2) regulates microRNA-10b via hypoxia-inducible factor 1-α-TWIST signaling networks in human breast cancer cells. *J Biol Chem* 2011;**286**:43475-43485.

28. Xia SF, Duan XM, Cheng XR, Chen LM, Kang YJ, Wang P, Tang X, Shi YH, Le GW. Role of miR-383 and miR-146b in different propensities to obesity in male mice. *J Endocrinol* 2017;**234**:201-216.

29. Song Y, Wu L, Li M, Xiong X, Fang Z, Zhou J, Yan G, Chen X, Yang J, Li Y Down-regulation of microRNA-592 in obesity contributes to hyperglycemia and insulin resistance. *Ebiomedicine* 2019;**42**:494-503.

30. Tani T, Orimo H, Shimizu A, Tsuruoka S. Development of a novel chronic kidney disease mouse model to evaluate the progression of hyperphosphatemia and associated mineral bone disease. *Sci Rep* 2017;**7**:2233.

31. Terai K, Nara H, Takakura K, Mizukami K, Sanagi M, Fukushima S, Fujimori A, Itoh H, Okada M. Vascular calcification and secondary hyperparathyroidism of severe chronic kidney disease and its relaion to serum phosphate and calcium levels. *Br J Pharmacol* 2009;**156**:1267-1278.

32. Diwan V, Brown L, Gobe GC. Adenine-induced chronic kidney disease in rats. *Nephrology* 2018;**23**:5-11.

33. Vervloet MG, Sezer S, Massy ZA, Johansson L, Cozzolino M, Fouque D. The role of phosphate in kidney disease. *Nat Rev Nephrol* 2017;**13**:27-38

34. Kuo H-C, Wong Henry S-C, Chang W-P, Chen B-K, Wu M-S, Yang KD, Hsieh KS, Hsu YW, Liu SF, Liu X, Chang WC. Prediction for Intravenous Immunoglobulin Resistance by Using Weighted Genetic Risk Score Identified From Genome-Wide Association Study in Kawasaki Disease. *Circ Cardiovasc Genet* 2017;**10**:e001625.

35. Wang H, Peng R, Wang J, Qin Z, Xue L. Circulating microRNAs as potential cancer biomarkers: the advantage and disadvantage. *Clin Epigenetics* 2018;**10**:59.

36. Devaux Y, Vausort M, McCann GP, Kelly D, Collignon O, Ng LL, Wagner DR, Squire IB. A Panel of 4 microRNAs Facilitates the Prediction of Left Ventricular Contractility after Acute Myocardial Infarction. *PLOS ONE* 2013;**8**:e70644.

37. Strand SH, Bavafaye-Haghighi E, Kristensen H, Rasmussen AK, Hoyer S, Borre M, Mouritzen P, Besenbacher S, Orntoft TF, Sorensen KD. A novel combined miRNA and methylation marker panel (miMe) for prediction of prostate cancer outcome after radical prostatectomy. *Int J Cancer* 2019;**145**:3445-3452.

38. Tian H, Chen S, Zhang C, Li M, Zheng H. MYC and hsa‐miRNA‐423‐5p as biomarkers in nasopharyngeal carcinoma revealed by miRNA‐mRNA‐pathway network integrated analysis. *Mol Med Rep* 2017;**16**:1039-1046.

39. Hammond E, Khurana A, Shridhar V, Dredge K. The Role of Heparanase and Sulfatases in the Modification of Heparan Sulfate Proteoglycans within the Tumor Microenvironment and Opportunities for Novel Cancer Therapeutics. *Front Oncol* 2014;**4**:195.

40. Thul PJ, Lindskog C. The human protein atlas: a spatial map of the human proteome. *Protein Sci* 2018;**27**:233-244.

41. Sala-Newby GB, George SJ, Bond M, Dhoot GK, Newby AC. Regulation of vascular smooth muscle cell proliferation, migration and death by heparan sulfate 6-O-endosulfatase1. *FEBS Lett* 2005;**579**:6493-6498.

42. Sahota AP, Dhoot GK. A novel SULF1 splice variant inhibits Wnt signalling but enhances angiogenesis by opposing SULF1 activity. *Exp Cell Res* 2009;**315**:2752-2764.

43. Nie B, Zhang S-y, Guan S-m, Zhou S-q, Fang X. Role of Wnt/β-Catenin Pathway in the Arterial Medial Calcification and Its Effect on the OPG/RANKL System. *Curr Med Sci* 2019;**39**:28-36.

44. Cha HJ, Kim HY, Kim HS. Sulfatase 1 mediated the attenuation of Ang II-induced hypertensive effects by CCL5 in vascular smooth muscle cells from spontaneously hypertensive rats. *Cytokine* 2018;**1**10:1-8.

45. Matsushita K, Wu Y, Pratt RE, Dzau VJ. Blockade of angiotensin II type 2 receptor by PD123319 inhibits osteogenic differentiation of human mesenchymal stem cells via inhibition of extracellular signal0regulated kinase signaling. *J Am Soc Hypertens* 2015;**9**:517-525.

46. Panizo S, Naves-Díaz M, Carrillo-López N, Martínez-Arias L, Fernández-Martín JL, Ruiz-Torres MP, Cannata-Andia JB. MicroRNAs 29b, 133b, and 211 Regulate Vascular Smooth Muscle Calcification Mediated by High Phosphorus. *J Am Soc Nephrol* 2016;**27**:824-834.

47. Boisvert NC, Holterman CE, Gutsol A, Coulombe J, Pan W, Alexander RT, Gray DA, Kennedy CR. Ubiquitin COOH-terminal hydrolase L1 deletion is associated with urinary α-klotho deficiency and perturbed phosphate homeostasis. *Am J Physiol Renal Physiol* 2018;**315**:F353-F363.

48. Liu L, Zeng P, Yang X, Duan Y, Zhang W, Ma C, Zhang X, Yang S, Li X, Yang J, Liang Y, Han H, Zhu Y, Han J, Chen Y. Inhibition of vascular calcification. *Arterioscler Thromb Vasc Biol* 2018;**38**:2382-2395.

49. Feng W, Zhang K, Liu Y, Chen J, Cai Q, Zhang Y, Wang M, Wang J, Huang H. Apocynin attenuates angiotensin II-induced vascular smooth muscle cells osteogenic switching via suppressing extracellular signal-regulated kinase 1/2. *Oncotarget* 2016;**7**:83588-83600.

50. Shin MK, Kim MK, Bae YS, Jo I, Lee SJ, Chung CP, Park YJ, Min do S. A novel collagen-binding peptide promotes osteogenic differentiation via Ca^{2+}/calmodulin-dependent protein kinase II/ERK/AP-1 signaling pathway in human bone marrow-derived mesenchymal stem cells. *Cell Signal* 2008;**20**:613-624.

Figure Legend

Figure 1. Establishing a 3-tier *in vitro* VC model and an animal model of uremic VC. (A) A schematic diagram showing the design of 3-tier *in vitro* calcification process. (B) Gross view of alizarin red staining of calcified VSMCs under stimuli of different extents. (C) Microscopic calcification nodules of calcified VSMCs. (D) *RUNX2* expression levels in control and calcified VSMCs of different severities (n = 4 per group). (E) Temporal trends in body weight among rats without and with CKD and/or high phosphate diet over 12 weeks (n = 6 per group). (F) Serum creatinine levels in control/CKD/CKD+HP groups (n = 6 per group). (G) Renal pathological findings based on H&E (upper row) and Masson trichrome stain (lower row) in control, CKD, and CKD+HP groups. Asterisks and arrowheads denote areas of tubular dilation and interstitial fibrosis, respectively. (H) Von Kossa stain of rat aortas in three groups. (I) Quantification of Von Kossa positive staining areas among control, CKD, and CKD+HP groups (n = 6 per group). (J) Serum calcium (left) and inorganic phosphate (right) levels in control, CKD, and CKD+HP groups (n = 6 per group). (K) Aortic *RUNX2* (upper) and osteocalcin (lower) expressions in control, CKD, and CKD+HP groups (n = 4 per group). Scale bar: C,G,H = 500 μm

*For comparisons > 2 groups, 1-way analysis of variance was used with Bonferroni's post-hoc adjustment. *P < 0.05, ** P < 0.01, ***P < 0.001.* ^{a}*P < 0.05,* ^{b}*P < 0.01,* ^{c}*P < 0.001 using Student's t-tests. Ca, calcium; CKD, chronic kidney disease; Cre, creatinine; Ctrl, control; D, vitamin D; DMEM, Dulbecco's modified Eagle medium; HP, high phosphate; I, indoxyl sulfate; OCN, osteocalcin; Pi, inorganic phosphate; T, tumor necrosis factor-α (TNF-α); VC, vascular calcification; VSMC, vascular smooth muscle cell*

Figure 2. Bioinformatic algorithm of screening for differentially expressed miRNAs and mRNAs based on microarray data.

Ctrl, control; GO, gene ontology; KEGG, Kyoto Encyclopedia of Genes and Genomes; miRNA, microRNA; VSMC, vascular smooth muscle cell

Figure 3. Heatmap of all tested miRNAs. (A) and mRNAs (B) in microarray experiments (n = 3 per *in vitro* group and 6 per *in vivo* group). Scatter plots (C) of directional changes in expression during *in vitro* calcification stimulus exposure (HP vs. control, left upper; HP+D vs. control, right upper; HP+I vs. control, left lower; HP+T vs. control, right lower) are shown, with yellow and green colored dots denoting positively and negatively deregulated candidates with higher-than threshold changes, respectively. Red dots indicate selected candidates from the final process, as explained in the text. The correlation extent amidst

filtered miRNA-mRNA pairs (up-regulated miRNAs/down-regulated mRNAs, D; down-regulated miRNAs/up-regulated mRNA, E) are illustrated based on the aggregated rank of target prediction derived from multiple individual rankings in miRNA target-prediction databases (lower values denoting mRNA as the more potent target of the paired miRNA). (F) Top GO terms enriched in differentially expressed mRNAs. Heat maps of the 16 differentially expressed miRNAs (G) and 14 differentially expressed mRNAs (H), which are potential targets of the 16 miRNAs, are shown. (I) Negatively deregulated miRNAs and their plausible target mRNAs, as well as involved biologic functions based on the database search results, are illustrated in a node plot.

CKD, chronic kidney disease; Ctrl, control; D, vitamin D; GO, Gene Ontology; HP, high phosphate; I, indoxyl sulfate; miRNA, microRNA; T, tumor necrosis factor-α (TNF-α); -log$_{10}$combined_p, minus log transformed (combined P values)

Figure 4. Validation results of the *in vitro, in vivo,* and the *ex vivo* uremic VC models as well as functional assays and luciferase-binding assay of miRNA/mRNAs. (A) In total, 5 of the 9 negatively deregulated miRNAs and 7 of the 14 positively deregulated mRNAs were validated in the *in vitro* model (n = 4 per group). (B) Among the 5 miRNAs, miR-378a-3p decreased significantly and progressively in aortas with increasing severity of VC, while among 7 mRNAs, *SULF1* exhibited rising changes in aortas with higher VC severity (n = 4 per group). (C) The paired miR-378a-3p and SULF1 were decreased and increased significantly in cultured calcified aortas, respectively, compared to controls (n = 4 per group).* denotes C-terminal fragments. (D) Gross (upper panel) and microscopic (lower panel) examination of alizarin red positive calcification nodules with and without transfection of the 4 miRNA mimics. (E) Calcium quantitation(left upper) results with and without miRNA mimics transfection, as well as the expression levels of osteocalcin (left lower), alkaline phosphatase (right upper), and *SULF1* (right lower) among each group (n = 3 per group). (F) Microscopic examination of Alizarin red positive calcification nodules with and without SULF1 siRNA transfection. (G) *SULF1* expression levels (upper) and calcium quantitation results (lower) with and without SULF1 siRNA transfection (n = 3 per group). (H) Base-pairing between miR-378a-3p and its predicted target, SULF1 (upper) and results from dual-luciferase binding assay between miR-378a-3p and SULF1 (lower) (n = 3 per group). Scale bar: D = 100 μm; F = 200 μm.

*For comparisons > 2 groups, 1-way analysis of variance was used with Bonferroni's post-hoc adjustment, while for 2-groups comparison, Student's t-tests were used. *P < 0.05, **P < 0.01, ***P < 0.001 compared to control group. ^{a}P < 0.05, ^{b}P < 0.01, ^{c}P < 0.001 using Student's t-tests. CKD, chronic kidney disease; Ctrl, control; D, vitamin D; DMEM,*

Dulbecco's modified Eagle medium; HP, high phosphate; I, indoxyl sulfate; NC, negative control; Neg miR, negative microRNA analog; siR, small interfering RNA; T, tumor necrosis factor-α (TNF-α); TR, transfection reagent; VC, vascular calcification; VSMC; vascular smooth muscle cells; 3'-UTR, 3'-untranslated region.

Figure 5. (A) Expression levels of the 4 candidate DEMis (miR-10b-5p, miR-195, miR-125b-2-3p, and miR-378a-3p) in rat VSMCs subjected to HP intracellularly and concurrently in their respective culture media (n = 3 per group). (B) Expression levels of the 4 DEMis in cultured rat aortas and in their respective culture media (n = 3 per group). (C) Expression levels of the 4 DEMis in the culture media of 2 types of human ASMCs (*left*, PCS-100; *right*, SI-354) (n = 3 per group). (D) Serum levels of the 4 DEMis among rats with increasing severity of uremic vascular calcification (n = 4 per group).

*For comparisons > 2 groups, 1-way analysis of variance was used with Bonferroni's post-hoc adjustment, while for 2-groups comparison, Student's t-tests were used. *P < 0.05, **P < 0.01, ***P < 0.001 compared to controls. ASMC, aortic smooth muscle cells; CKD, chronic kidney disease; Ctrl, control; DEMi, differentially expressed microRNA; HP, high phosphate; VSMC, vascular smooth muscle cell.*

Figure 6. Clinical validation results in two cohorts. (A) Circulating miR-125b-2-3p (upper) and miR-378a-3p (lower) levels in ESRD patients with (n = 68) and without VC (n = 28) and (B) with different severities of VC (for category 1, 2, and 3, n = 34, 24, and 10, respectively; compared between groups using one-way analysis of variance) are shown. (C) Circulating *SULF1* levels in ESRD patients with (n = 68) and without VC (n = 28) (left) or with different severities of VC (for category 1, 2, and 3, n = 34, 24, and 10, respectively; compared between groups using one-way analysis of variance) (right). (D) ROC curves and (E) precision-recall curves based on 5 regression models associated with uremic VC presence incorporating different model components, with AUROC values provided in the text. (F) Circulating miR-125b-2-3p (upper) and miR-378a-3p (lower) levels in non-dialysis CKD patients with (n = 36) and without VC (n = 23) and (G) with different severities of VC (for category 1, 2, and 3, n = 19, 11, and 6, respectively; compared between groups using one-way analysis of variance) are shown. (H) Circulating *SULF1* levels in non-dialysis CKD patients with (n = 36) and without VC (n = 23) (left) or with different severity of VC (for category 1, 2, and 3, n = 19, 11, and 6, respectively; compared between groups using one-way analysis of variance) (right). (I) A graphical illustration of the main findings and clinical applications of this study

*For comparisons > 2 groups, 1-way analysis of variance was used, while for 2-groups comparison, Student's t-tests were used. *P < 0.05, ***P < 0.001 compared to AAC absence*

group. AAC, aortic arch calcification; AUROC, area under the receiver-operating-characteristics curve; CKD, chronic kidney disease; ESRD, end-stage renal disease; GO, gene Ontology; KEGG, Kyoto Encyclopedia of Genes and Genomes; miRs, microRNAs; ROC, receiver-operating-characteristics curve; VC, vascular calcification; VSMC, vascular smooth muscle cell.

Table 1. Clinical features of end-stage renal disease participants (n=96)

Features	No AAC (n=28)	AAC (+) (n=68)	*p-value*	AAC category			*p-value*
				1 (n=34)	2 (n=24)	3 (n=10)	
Demographic profile							
Age (years)	55.1 ± 14.7	68.9 ± 14.2	*<0.001*	64.4 ± 17	72.6 ± 10	75.3 ± 5.7	*<0.001*
Gender (male%)	12 (43)	32 (47)	*0.711*	17 (50)	12 (50)	3 (30)	*0.689*
Duration of dialysis (years)	5.1 ± 2.9	5.8 ± 4.3	*0.401*	5.5 ± 4.6	6.1 ± 3.1	6.3 ± 6.1	*0.756*
Comorbidity							
Diabetes mellitus (%)	5 (18)	29 (43)	*0.021*	16 (47)	7 (29)	6 (60)	*0.030*
Hypertension (%)	24 (86)	63 (93)	*0.294*	30 (88)	23 (96)	10 (100)	*0.430*
Heart failure (%)	6 (21)	20 (29)	*0.429*	10 (29)	8 (33)	2 (20)	*0.744*
CAD (%)	8 (29)	30 (44)	*0.160*	11 (32)	13 (54)	6 (60)	*0.111*
PVD (%)	0 (0)	6 (9)	*0.107*	1 (3)	3 (13)	2 (20)	*0.062*
Old cerebrovascular event (%)	2 (7)	8 (12)	*0.506*	3 (9)	2 (8)	3 (30)	*0.205*
*Physical parameter**							
BMI (kg/m^2)	25.1 ± 4.2	23.4 ± 3.9	*0.214*	23.9 ± 4	22.4 ± 4	24 ± 3.4	*0.286*
Systolic BP (mmHg)	135.6 ± 18.4	140.2 ± 22.4	*0.555*	140.2 ± 19.7	144.3 ± 27.8	130.6 ± 14.3	*0.382*
Diastolic BP (mmHg)	72.9 ± 8.5	71.4 ± 12.9	*0.741*	73.7 ± 14.4	71.2 ± 11.8	64.4 ± 7.1	*0.223*
Medication							
Aspirin (%)	4 (14)	16 (24)	*0.316*	8 (24)	5 (21)	3 (30)	*0.718*
Clopidogrel (%)	2 (7)	11 (16)	*0.244*	1 (3)	8 (33)	2 (20)	*0.005*
Statin (%)	4 (14)	4 (6)	*0.179*	2 (6)	2 (8)	0 (0)	*0.491*
Calcium-based phosphate binders (%)	21 (75)	53 (78)	*0.758*	28 (82)	19 (79)	6 (60)	*0.521*
Active vitamin D (%)	11 (39)	25 (37)	*0.819*	12 (35)	11 (46)	2 (20)	*0.558*

Laboratory paramters							
Hemoglobin (mg/dL)	10.3 ± 1.2	10.7 ± 1.7	*0.242*	10.5 ± 1.3	10.8 ± 1.8	11.3 ± 2.3	*0.330*
Albumin (g/dL)	3.8 ± 0.3	3.8 ± 0.4	*0.752*	3.9 ± 0.3	3.7 ± 0.5	3.8 ± 0.3	*0.361*
Calcium (mg/dL)	9.3 ± 0.9	9.2 ± 0.8	*0.805*	9.2 ± 0.8	9.4 ± 0.9	9.2 ± 0.6	*0.820*
Phosphate (mg/dL)	5.3 ± 1.2	5 ± 1.3	*0.317*	5.1 ± 1.4	5 ± 1.3	5 ± 1.3	*0.749*
Ca-P product	49.6 ± 12.5	46.6 ± 12.7	*0.288*	46.6 ± 12.5	46.7 ± 13.4	46.2 ± 12.8	*0.770*
iPTH (pg/mL)	363.3 ± 330.6	444.3 ± 393.1	*0.340*	388.5 ± 322.8	577.5 ± 482.9	313.9 ± 306.8	*0.116*
Total cholesterol (mg/dL)*	171.6 ± 43.7	154.6 ± 32.5	*0.163*	154.1 ± 35.3	153.6 ± 26.4	159 ± 38.4	*0.548*
Triglyceride (mg/dL)*	183.8 ± 122.9	151.8 ± 106.1	*0.406*	153.2 ± 111.1	141.7 ± 97.6	171.3 ± 116	*0.75*
HDL (mg/dL)*	43.9 ± 15	41.4 ± 13	*0.594*	42.3 ± 12.2	42.7 ± 15	35.1 ± 9.1	*0.401*
LDL (mg/dL)*	102.2 ± 34.7	87 ± 24.5	*0.102*	85.9 ± 25.7	86.3 ± 22.4	92.8 ± 27.2	*0.359*

* n = 77 (No AAC vs. AAC = 9 vs. 68)

Abbreviations: AAC, aortic arch calcification; BMI, body mass index; BP, blood pressure; CAD, coronary artery disease; HDL, high density lipoprotein; iPTH, intact parathyroid hormone; LDL, low density lipoprotein; PVD, peripheral vascular disease

Table 2. Multiple regression analyses with stepwise backward variable selection of factors independently associated with vascular calcification among the recruited end-stage renal disease patients (n = 77)

Factors	Odds ratio	95% confidence interval	*p-value*
Model 1: Clinical variables			
NA*	-	-	-
Model 2: Clinical variables + serum SULF1			
SULF1	1.419	1.044 – 1.928	*0.025*
Model 3: Clinical variables + serum miR-125b-2-3p			
miR-125b-2-3p	0.939	0.896 – 0.984	*< 0.001*
Model 4: Clinical variables + serum miR-378a-3p			
miR-378a-3p	0.854	0.769 – 0.949	*0.003*
Model 5: Clinical variables + serum SULF1 + miR-125b-2-3p and miR-378a-3p			
miR-378a-3p	0.83	0.706 – 0.975	*0.023*
SULF1	1.466	1.004 – 2.217	*0.048*

** None of the 4 variables was significant in the model.*
NA, not available
Model 1: including age, gender, diabetes mellitus, and use of clopidogrel
Model 2: model 1 components plus serum SULF1
Model 3: model 1 components plus serum miR-125b-2-3p
Model 4: model 1 components plus serum miR-378a-3p
Model 5: model 1 components plus serum SULF1, miR-378a-3p, and miR-125b-2-3p

Figure 1

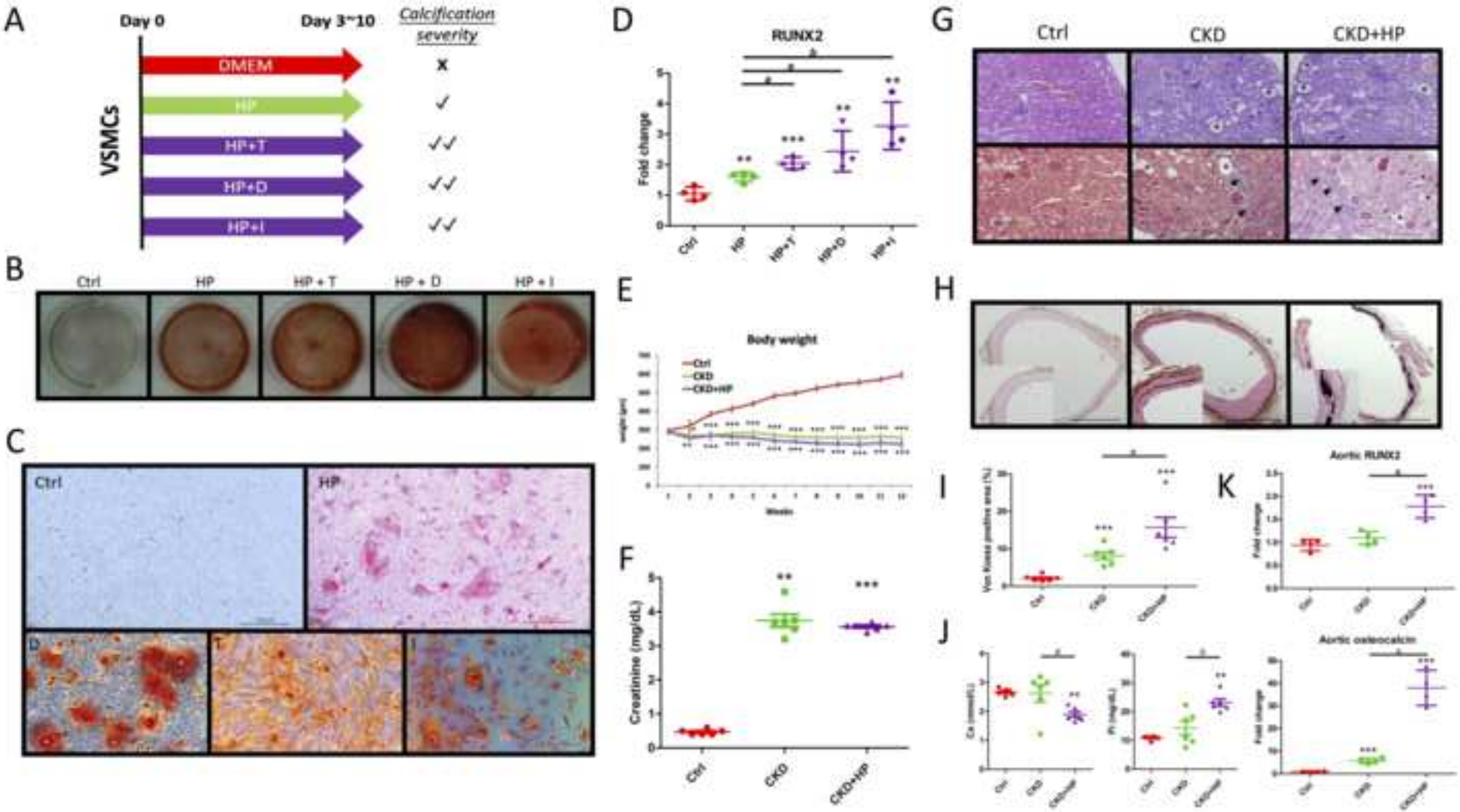

Figure 2

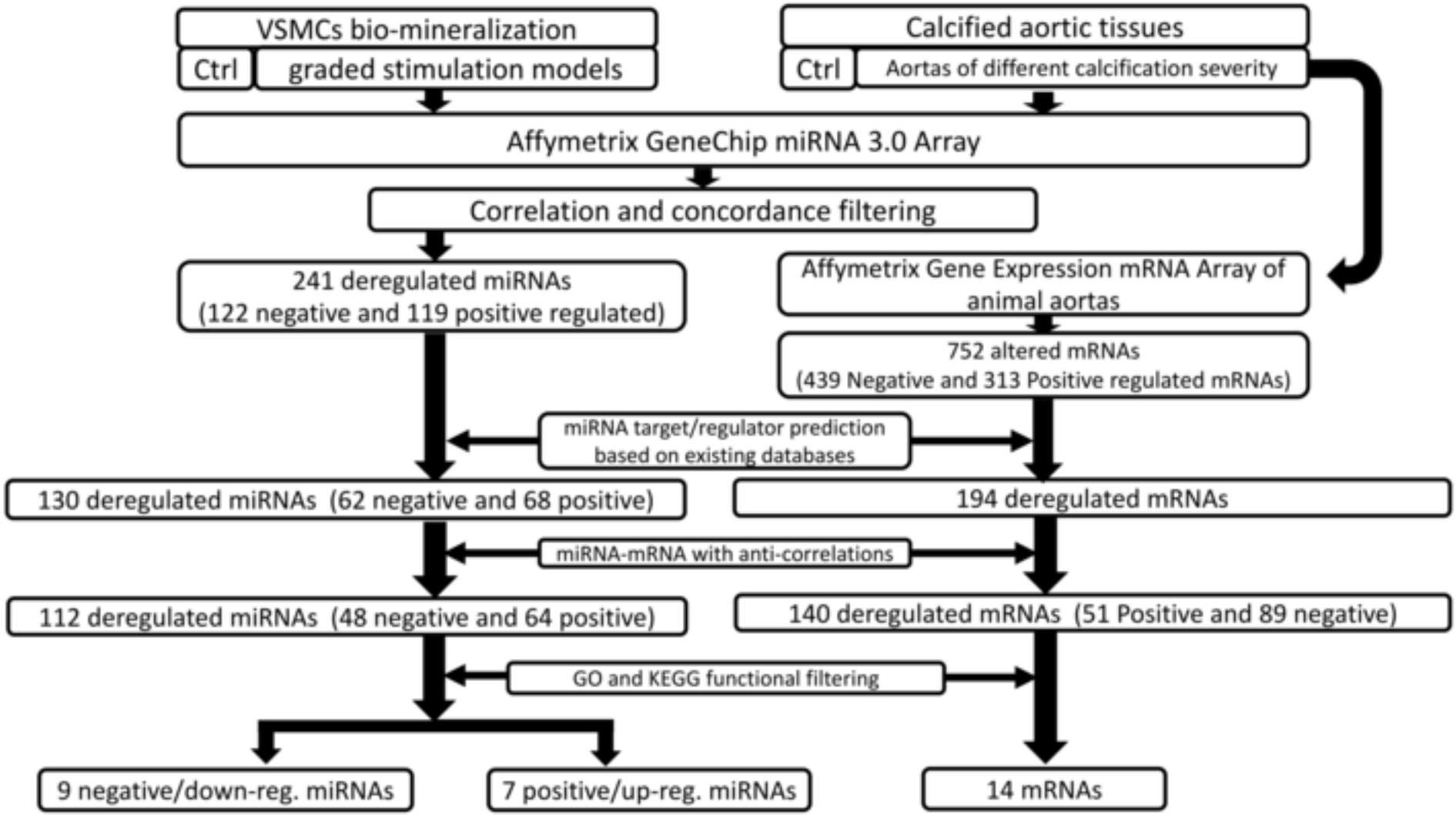

Figure 3

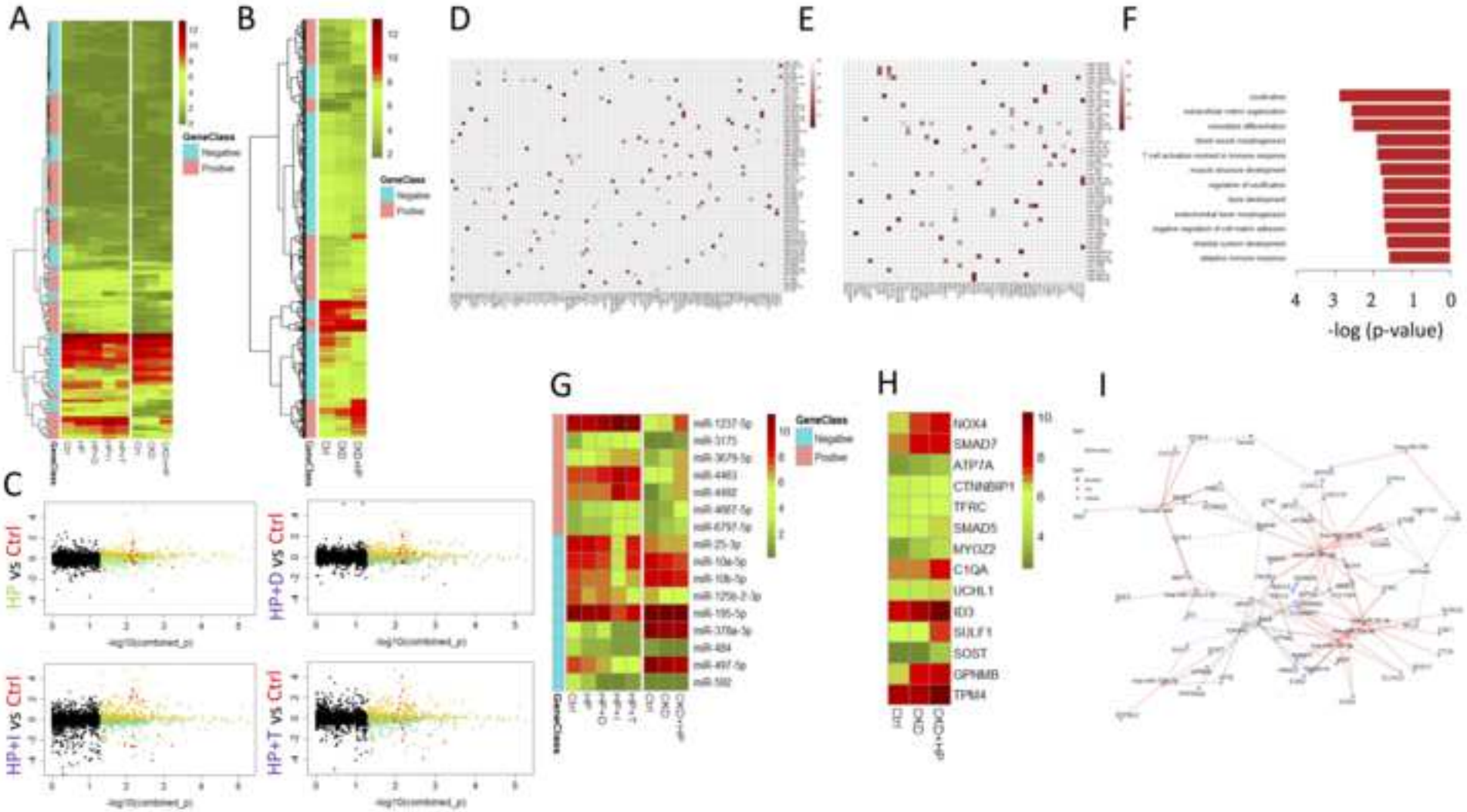

Figure 4

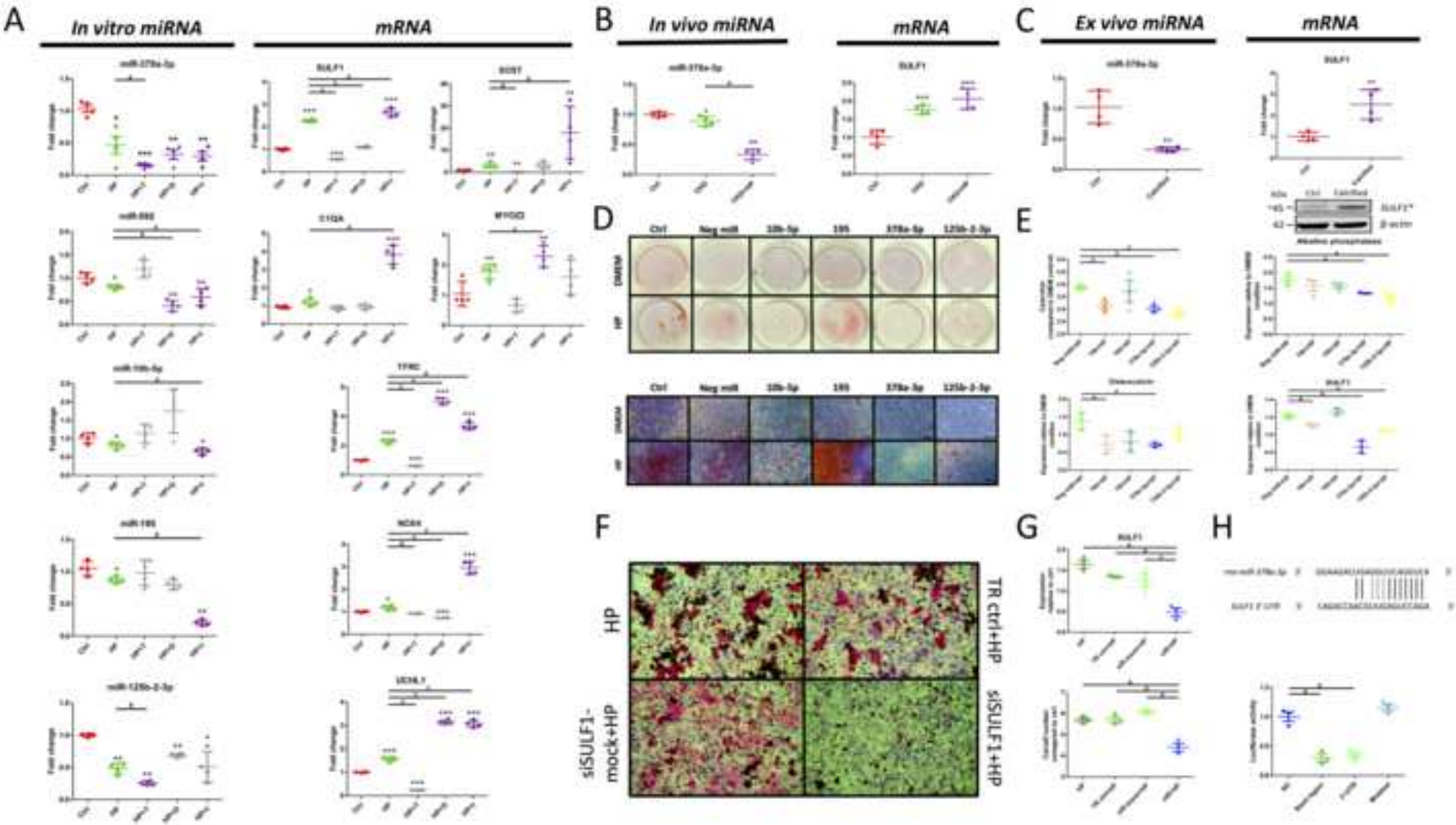

Figure 5

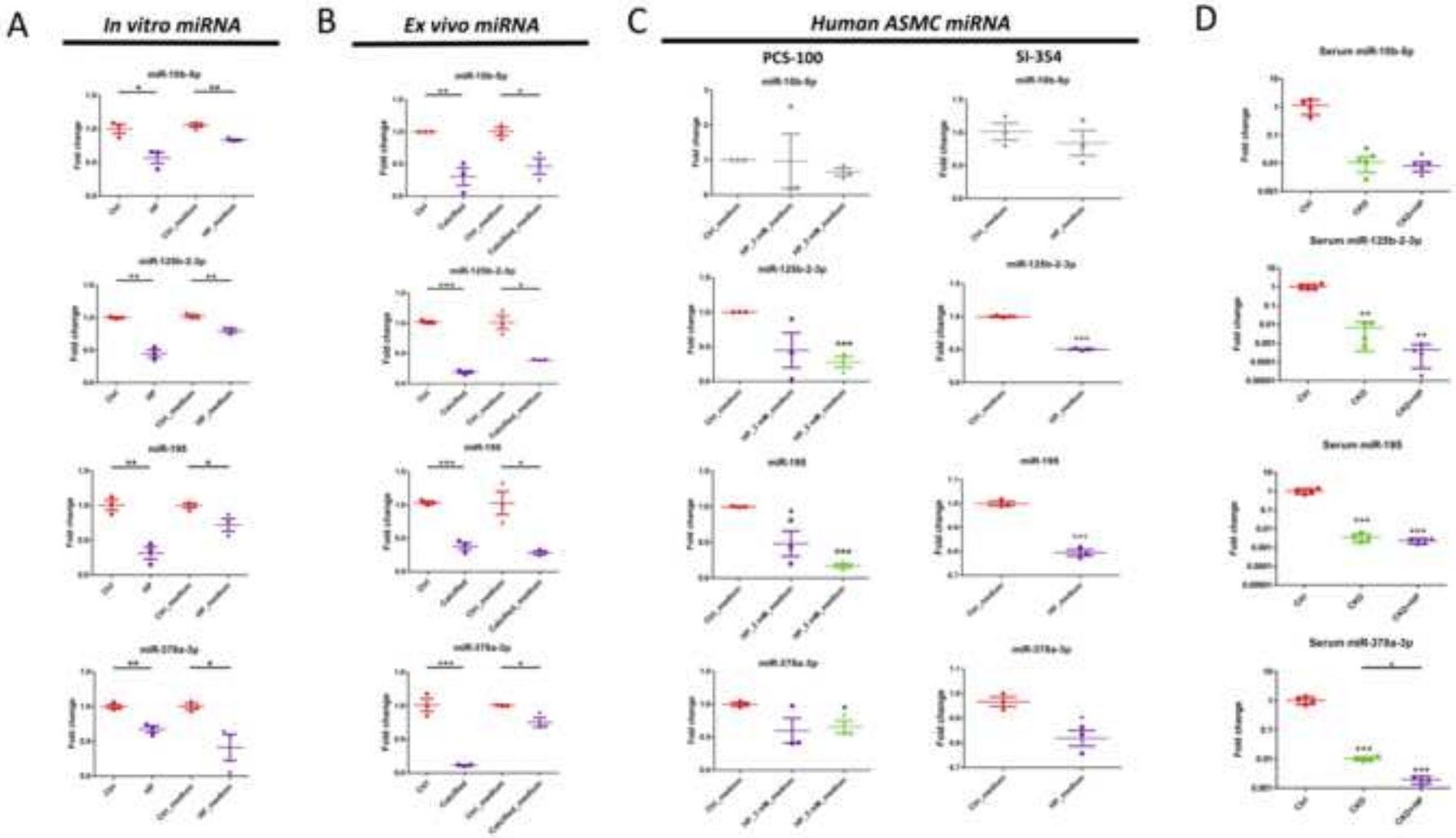

Figure 6

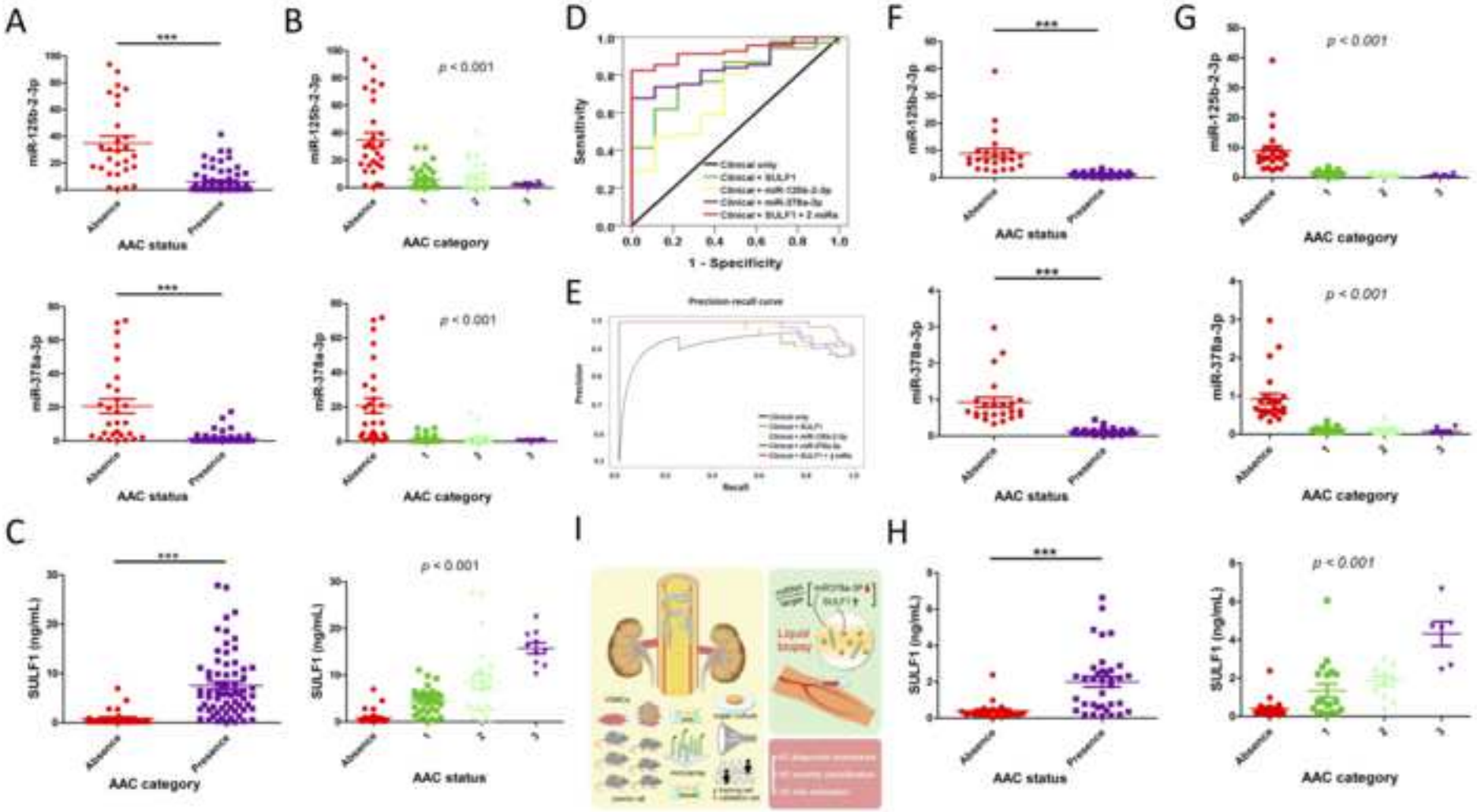

Graphical Abstract